NASA/CR—2002-211992

Performance of a Model Rich Burn-Quick Mix-Lean Burn Combustor at Elevated Temperature and Pressure

Christopher O. Peterson, William A. Sowa, and G.S. Samuelsen
University of California, Irvine, Irvine, California

December 2002

The NASA STI Program Office . . . in Profile

Since its founding, NASA has been dedicated to the advancement of aeronautics and space science. The NASA Scientific and Technical Information (STI) Program Office plays a key part in helping NASA maintain this important role.

The NASA STI Program Office is operated by Langley Research Center, the Lead Center for NASA's scientific and technical information. The NASA STI Program Office provides access to the NASA STI Database, the largest collection of aeronautical and space science STI in the world. The Program Office is also NASA's institutional mechanism for disseminating the results of its research and development activities. These results are published by NASA in the NASA STI Report Series, which includes the following report types:

- TECHNICAL PUBLICATION. Reports of completed research or a major significant phase of research that present the results of NASA programs and include extensive data or theoretical analysis. Includes compilations of significant scientific and technical data and information deemed to be of continuing reference value. NASA's counterpart of peer-reviewed formal professional papers but has less stringent limitations on manuscript length and extent of graphic presentations.

- TECHNICAL MEMORANDUM. Scientific and technical findings that are preliminary or of specialized interest, e.g., quick release reports, working papers, and bibliographies that contain minimal annotation. Does not contain extensive analysis.

- CONTRACTOR REPORT. Scientific and technical findings by NASA-sponsored contractors and grantees.

- CONFERENCE PUBLICATION. Collected papers from scientific and technical conferences, symposia, seminars, or other meetings sponsored or cosponsored by NASA.

- SPECIAL PUBLICATION. Scientific, technical, or historical information from NASA programs, projects, and missions, often concerned with subjects having substantial public interest.

- TECHNICAL TRANSLATION. English-language translations of foreign scientific and technical material pertinent to NASA's mission.

Specialized services that complement the STI Program Office's diverse offerings include creating custom thesauri, building customized databases, organizing and publishing research results . . . even providing videos.

For more information about the NASA STI Program Office, see the following:

- Access the NASA STI Program Home Page at ***http://www.sti.nasa.gov***

- E-mail your question via the Internet to help@sti.nasa.gov

- Fax your question to the NASA Access Help Desk at 301–621–0134

- Telephone the NASA Access Help Desk at 301–621–0390

- Write to:
  NASA Access Help Desk
  NASA Center for AeroSpace Information
  7121 Standard Drive
  Hanover, MD 21076

NASA/CR—2002-211992

Performance of a Model Rich Burn-Quick Mix-Lean Burn Combustor at Elevated Temperature and Pressure

Christopher O. Peterson, William A. Sowa, and G.S. Samuelsen
University of California, Irvine, Irvine, California

Prepared under Grant NAG3–1110

National Aeronautics and
Space Administration

Glenn Research Center

December 2002

Available from

NASA Center for Aerospace Information
7121 Standard Drive
Hanover, MD 21076

National Technical Information Service
5285 Port Royal Road
Springfield, VA 22100

Available electronically at http://gltrs.grc.nasa.gov

TABLE OF CONTENTS

PAGE

LIST OF SYMBOLS

C_x = concentration of constituent x in ppm

EI(X) = Emissions Index for X (gms X / kg fuel)

k = rate of reaction

M_f = molecular weight of fuel

M_p = molecular weight of products of combustion

n_C = number of atoms of carbon in one molecule of fuel

P = pressure

R = Universal Gas Constant

r = hydrogen to carbon atom ratio in fuel molecule

T = absolute temperature

Φ = equivalence ratio

η = combustion efficiency

LIST OF SUBSCRIPTS

eq = equilibrium

lz = lean zone

rz = rich zone

1.0 INTRODUCTION

1.1 OVERVIEW

As gas turbine technology advances into the 21st century, combustion engineers are faced with the challenge of achieving higher compression ratios and higher turbine inlet temperatures in aero gas turbine engines. At the same time, as interest in pollutant emissions from gas turbines increases, combustion engineers are also required to consider new means for pollutant reduction.

In the past, aero gas turbine engine designers have sacrificed emissions to attain greater flight speeds and altitudes. For today's aero gas turbine engines, it is necessary to reduce these emissions, while at the same time, maintaining these same speeds and altitudes. In some European countries, airlines are being taxed for NO_X emissions in their airspace. Concern for pollutant reduction is particularly strong for the next generation of aircraft, represented by the High Speed Civil Transport, which is being designed to fly at stratospheric altitudes. In the stratosphere, NO_X emissions could contribute to ozone depletion. (Johnston, 1971)

To achieve this reduction in NO_X emissions, engine designers have been challenged to evaluate various combustor configurations. One promising configuration is the three-stage RQL combustor. In the RQL (rich burn - quick mix - lean burn) combustor, air is mixed with the fuel in two stages. In the primary zone of the combustor, a fraction of the total air is reacted with the fuel to form a fuel rich combustion mixture. By operating rich of stoichiometery, the flame temperature is reduced and an active pool of hydrocarbon is produced which can reduce NO formed. Downstream, the remaining air is added to the fuel rich product mixture via dilution jets to

form a fuel lean mixture in the secondary zone. Operating lean of stoichiometric keeps the combustion temperature low and also eliminates carbon monoxide (CO) and unburnt hydrocarbons (UHC).

To date, the reduction of NO_X from staged RQL type combustors operating at atmospheric, low temperature inlet conditions has been well documented. Staged combustion has been demonstrated successful at reducing thermal and fuel NO at atmospheric conditions with no air preheat (Yamagishi, et al, 1975; Beér, et al, 1982), and at atmospheric conditions with air preheat up to 600 K (Sadakata, et al, 1981).

However, little information exists for the RQL's low NO_X potential when operating at temperatures and pressures that correspond to actual gas turbine engines. A full evaluation of the RQL, for use in stationary and aero applications, requires a systematic study of the effects of current, as well as futuristic, operating conditions on the emissions of NO_X and combustion efficiency.

This study seeks to establish the effects of typical HSCT operating conditions on emissions production by examining the roles inlet temperature, pressure, reference velocity, rich zone equivalence ratio, and lean zone equivalence ratio play in the production of emissions, particularly NO_X, from a model rich burn - quick mix - lean burn combustor in the fuel rich zone (first stage) and the fuel lean zone (third stage). Mixing within the quick mix zone (second stage) at realistic operating conditions is addressed in a separate thesis (Kroll, 1993).

1.2 GOALS AND OBJECTIVES

The two main goals of this research are to characterize the performance of the RQL combustor at elevated inlet temperatures and pressures and to

determine the significance of various operating parameters on NO_X emissions and combustion efficiency. To achieve these goals, four objectives were established.

1. Modify an existing testing facility in order to make it capable of simulating actual gas turbine engine combustor operating conditions.

2. Develop a model RQL combustor that would simulate the plenum feed characteristic of practical gas turbine combustor hardware.

3. Obtain exit plane emissions data for the RQL combustor operated under various conditions.

4. Identify where NO_X production is occuring by operating the model RQL combustor at realistic conditions and obtain emissions profiles at the exit of the rich zone and entrance of the lean zone as well as exit plane measurements.

2.0 BACKGROUND

2.1 GAS TURBINE ENGINES

2.1.1 AERO GAS TURBINES

Aero gas turbines do not vary greatly in their general design constraints. They all operate on a limited range of fuels and produce power for one type of application, usually thrust. Figure 2.1 provides an illustration of a typical aero gas turbine, the General Electric J79 turbojet engine. Turbojets represent air-breathing engines, which continuously draw air from the atmosphere, compress it, add energy in the form of heat, and then expand it in order to convert a portion of the added energy to shaft work which can run the compressor and produce thrust. The sources of energy for these engines are liquid hydrocarbon fuels. Figure 2.2 provides a schematic of the basic internal arrangement of the typical aero gas turbine engine.

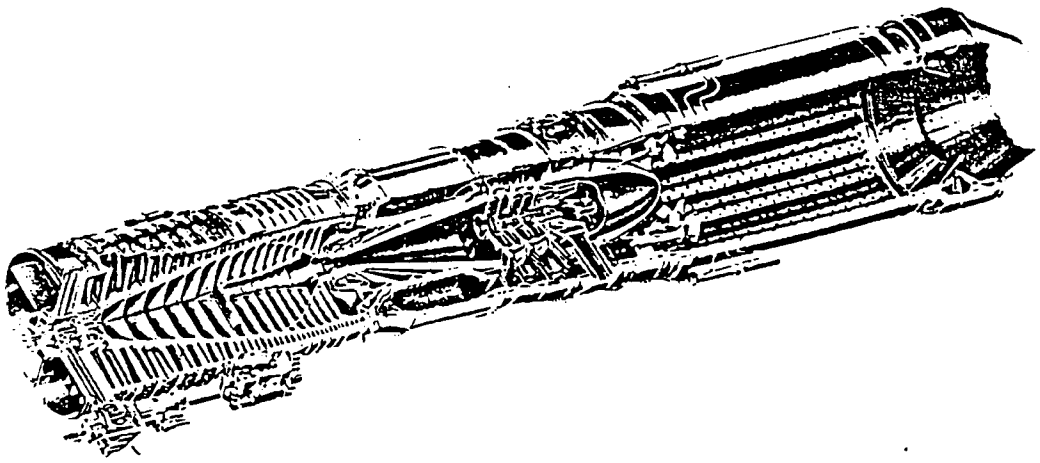

Figure 2.1 - General Electric J79 Turbojet Engine

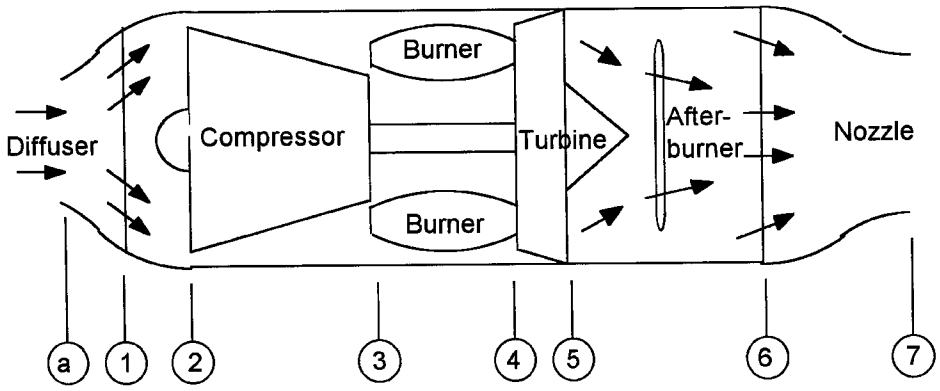

Figure 2.2 - Schematic of Aero Gas Turbine Engine

The numbers assigned to the various points within the engine are based on the system established in MIL-E-5007 (Mattingly, 1987). This system can be applied to all forms of aircraft engine and divides the engine into commonly numbered major zones. Between each zone, the air passing through the engine undergoes a specific process. These various processes (see Figure 2.2) can be broken down into the following steps (Peterson & Hill, 1965):

a - 1: From far upstream, where the velocity of the air relative to the engine is the flight velocity, the air is brought to the intake, usually with some acceleration or deceleration.

1 - 2: The velocity is decreased as the air is carried to the compressor inlet through the inlet diffuser and ducting system.

2 - 3: The air is compressed in the dynamic compressor. The compression ratio for the compressor is a fixed value usually

predetermined to provide a minimum fuel consumption to thrust ratio for a specific flight velocity.

3 - 4: The air is "heated" by the mixing and burning of fuel in the air.

4 - 5: The air is expanded through the turbine to obtain power to drive the compressor.

5 - 6: The air may or may not be further "heated" by the addition and burning of more fuel in an afterburner.

6 - 7: The air is accelerated and exhausted through the exhaust nozzle to produce thrust.

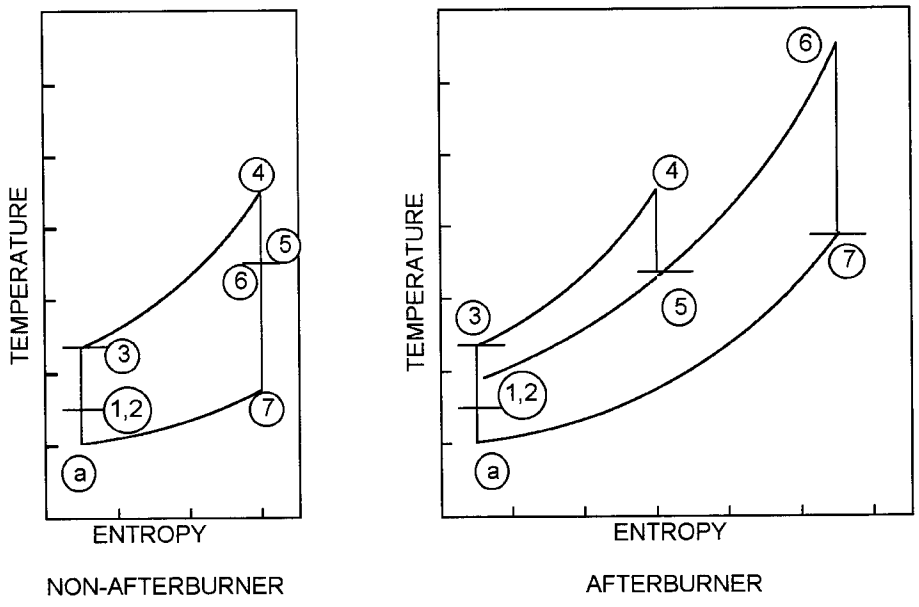

Figure 2.3 - Thermodynamic Representation of Aero Gas Turbine Engine

These processes, with and without the addition of the afterburner are presented on an entropy vs. temperature thermodynamic chart in Figure 2.3. From these charts it is clear that, at the entrance to the combustor, the air is at an elevated temperature and pressure. It is also clear that these combustor inlet conditions are dependent on both the flight conditions of the engine (point a), and the compression ratio of the dynamic compressor (points 2 to 3). For a given compression ratio, the inlet temperature and pressure to the combustor will increase with increases in atmospheric air density and temperature. Therefore, at take off and early climb, when the air brought into the engine is at 101.3 kPa and 295 K, the inlet conditions to the combustor will be much higher than at high altitude cruise, where the air density and temperature is much lower. Similarly, for a given flight condition, the inlet conditions to the combustor will be higher for a compressor with a higher compression ratio.

The inlet conditions to the combustor are also dependent on the aircraft flight speed. The total pressure of the air entering the engine is the sum of the static pressure and the pressure due to ram. For flight speeds less than Mach 1.5, the pressure due to ram is negligible. However, for speeds greater than Mach 1.5, the pressure due to ram increases with air speed as depicted in Figure 2.4. (Pratt &Whitney, 1988)

Air inlet temperature can also rise as a result of ram. The total temperature of a moving gas is the ambient temperature plus the rise due to ram effect. The relation between temperature and air speed is illustrated in Figure 2.5. (Pratt & Whitney, 1988)

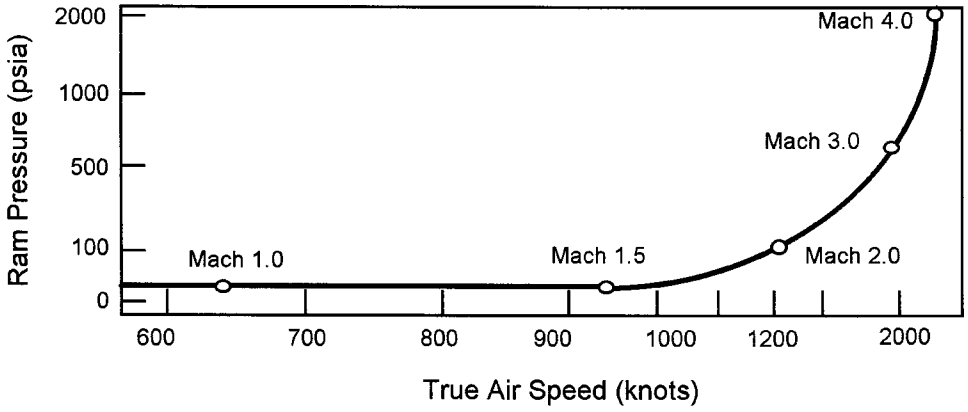

Figure 2.4 - Ram Pressure vs. Airspeed

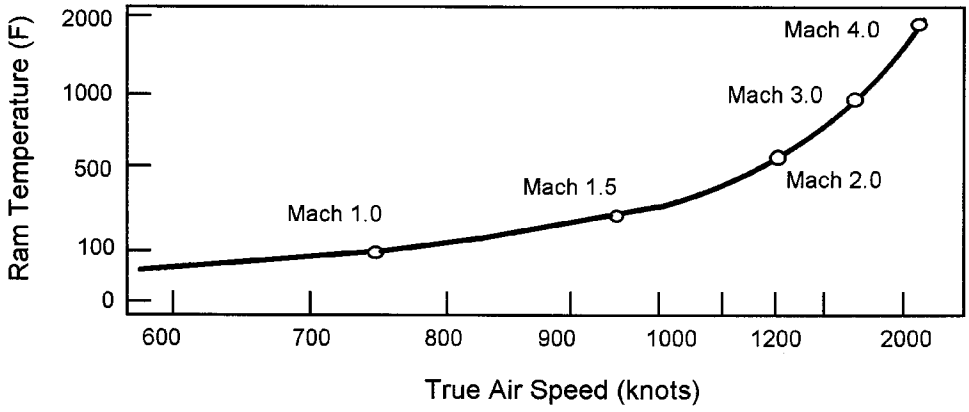

Figure 2.5 - Temperature vs. Airspeed

Modern aircraft typically operate at altitudes between 7500 m to 11000 m and have compression ratios between 15 and 20 (Mattingly, 1987). At this altitude the ambient air has roughly a pressure of 27.5 kPa (30% sea level) and an absolute temperature of 236 K (80% sea level) (ICAO, 1958).

Since the flight speed is less than Mach 1, ram has little effect and the combustor inlet conditions usually approach 620 kPa and 700 K.

At high altitude cruise, turbojets only operate at 70 to 80% maximum thrust. At take off and low altitude climb, typical turbojets operate at 100% thrust. The ambient air is 101.3 kPa and 294 K. Again, since the air speed is low, ram effects can be neglected. For these operating conditions, the combustor inlet conditions can increase to almost 2070 kPa and 820 K.

Futuristic aircraft, such as the High Speed Civil Transport, that will operate at stratospheric altitudes (around 18500 m) and at supersonic velocities (Mach 2 to 3) can achieve this increase in speed with greater compression ratios. At an altitude of 18500 m, the ambient air will have a temperature of 222 K and a static pressure of 5.0 kPa. At an air speed that exceeds Mach 1.0, the effects of ram have to be considered. At Mach 2.0, for example, the inlet air to the engine will have a pressure of 41 kPa and a temperature of 340 K. For a compression ratio of 25, this will result in combustor inlet conditions of 1033 kPa and 900 K.

2.2 EMISSIONS FROM GAS TURBINE COMBUSTORS

2.2.1 NOx

Of the many harmful pollutants found in gas turbine emissions, oxides of nitrogen, or NO_X, require the most attention. At most operating conditions, the bulk (in excess of 90%) of NO_X produced is in the form of NO.

There are four processes by which NO can be formed during combustion reactions: thermal NO production, prompt NO production, NO produced by fuel-bound nitrogen (Brady et al., 1991) and low temperature NO (Westbrook, 1992). In applications involving practical gas turbine

combustors, thermal NO is the most significant of these processes, with Prompt NO being the only other significant contributor.

Thermal NOx is produced by oxidation of atmospheric nitrogen in post flame gases. The formation of thermal NO can be illustrated by the three reactions composing the extended Zeldovich mechanism (Miller & Bowman, 1991; Glassman, 1987; Samuelsen, 1975; Zeldovich, 1946) listed on the following page.

$$N_2 + O \Leftrightarrow NO + N$$

$$N + O_2 \Leftrightarrow NO + O$$

$$N + OH \Leftrightarrow NO + H$$

Since the first of these three reactions is the rate limiting reaction, the Zeldovich method can be simplified to:

$$d[NO]/dt = \text{const}([N_2][O] \exp(-E/RT))$$

In this simplified model, NO production increases linearly with the local concentrations of N_2 and O and exponentially with reaction temperature. The temperature dependence of this model becomes important for temperatures exceeding 1900 K. The significance of the 1900 K reaction temperature is related to the breaking of the triple bond in molecular nitrogen (N_2) which must occur in order for the first reaction of the Zeldovich mechanism to proceed.

Prompt NO, which can also be formed in gas turbine combustion processes, is produced by high-speed reactions at the flame front. Unfortunately, the specific mechanisms of prompt NO are not well understood. Attempts to characterize the formation of prompt NO are complicated by the presence of super equilibrium O-atom concentrations in and near the primary combustion zone which temporarily accelerate the production of thermal NO by the Zeldovich mechanism. (Herberling, 1976; Fenimore, et al., 1987; Miller & Bowman, 1991) This sudden increase in NO can be mislabeled as prompt NO.

The basis for the prompt NO mechanism is believed to be reactions involving fragmented hydrocarbons attacking atmospheric nitrogen (Fenimore, 1971 and Haynes, et al., 1975). The most significant of these reactions are considered to be:

$$CH + N_2 \Leftrightarrow HCN + N$$

$$CH_2 + N_2 \Leftrightarrow HCN + NH$$

$$CH_2 + N_2 \Leftrightarrow H_2CN + N$$

$$C + N_2 \Leftrightarrow CN + N$$

An additional component of the prompt mechanism may parallel the mechanism for fuel-nitrogen derived NO with the HCN eventually forming an ammonia species (Haynes, et al., 1975). The final step of the prompt NO mechanism involves the oxidation of amines or cyano species to NO (Miller and Bowman, 1990). Since, at present, a detailed understanding of

the prompt NO mechanism is unavailable, it is unclear whether the prompt NO mechanism plays a significant role in the formation of NO_X in gas turbine engines operating at realistic conditions.

2.2.2 CO AND UHC

Carbon monoxide (CO) is a product of incomplete combustion and can be formed as a result of inadequate burning rates in the primary zone, insufficient residence times, inadequate mixing of the fuel or quenching of the primary zone post flame products by dilution air. (Lefebvre, 1983) The oxidation of CO to CO_2 is dependent on residence time and flame temperature. For high temperatures, the oxidation process revolves around the reaction:

$$CO + OH \rightarrow CO_2 + H$$

which is a fast reaction. For lower temperatures, the oxidation process revolves around the reaction:

$$CO + H_2O \rightarrow CO_2 + H_2$$

Unburned hydrocarbons, or UHC, include fuel that emerges from the exit of the combustor as either liquid or vapor, and products of the thermal degradation of the parent fuel into species of lower molecular weight, such as methane. The formation of UHC can be linked to poor atomization, inadequate burning rates, or quenching from dilution air.

2.3 MINIMIZATION OF EMISSIONS FROM GAS TURBINE ENGINES

One of the most significant factors controlling emissions from gas turbine engines is the temperature of the combustion products, which in turn, is dependent on the equivalence ratio. This dependence of flame temperature on equivalence ratio is illustrated for reactions involving air and Jet-A in Figure 2.6. This plot is based on a NASA equilibrium code and assumes both equilibrium and a perfectly mixed combustion process. This temperature maximizes slightly rich of stoichiometry (Φ = 1.1) and steadily decreases in value for equivalence ratios off stoichiometry.

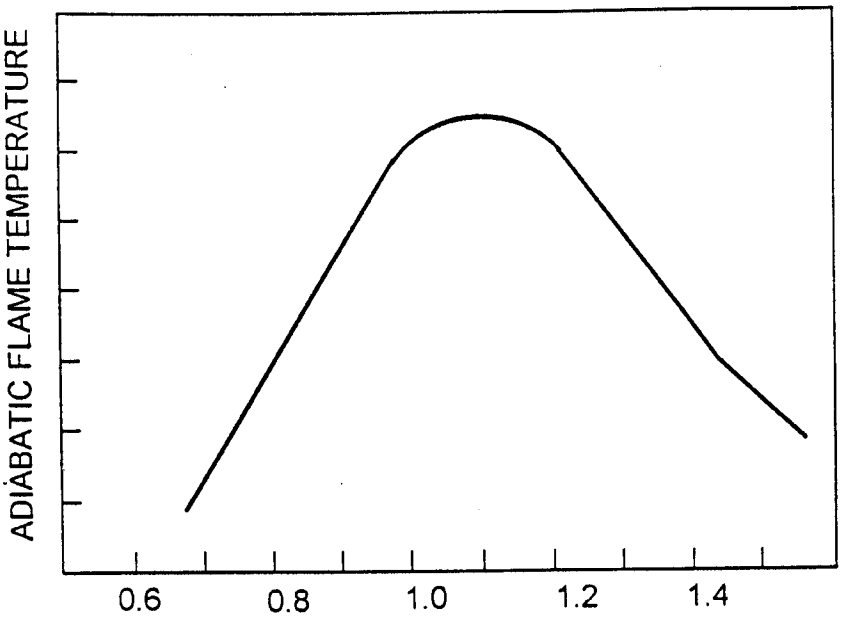

Figure 2.6 - Flame Temperature vs. Equivalence Ratio

As a result of the temperature dependence on the reaction rates for many of the reactions which occur in the combustion region, the combustion emissions of NO_X can also be shown to be dependent on equivalence ratio. At equivalence ratios approaching 1.0, the flame temperature exceeds the 1900 K critical value and the concentration of NO begins to climb. The emissions of CO and UHC are also dependent on equivalence ratio. For

fuel rich mixtures, the presence of excess fuel results in incomplete combustion. Unburned fuel, in the form of either liquid or vapor, is exhausted out of the combustor along with other indicators of incomplete combustion such as CO. Thus, as the equivalence ratio increases past stoichiometry, the concentration of CO and UHC increase. For fuel lean reactions, excess oxygen results in the complete oxidation of the majority of the CO and hydrocarbon species. Thus, as the equivalence ratio decreases past stoichiometry, the concentration of CO and UHC approaches equilibrium concentration levels. The dependence of these various emission concentrations on equivalence ratio are illustrated in Figure 2.7.

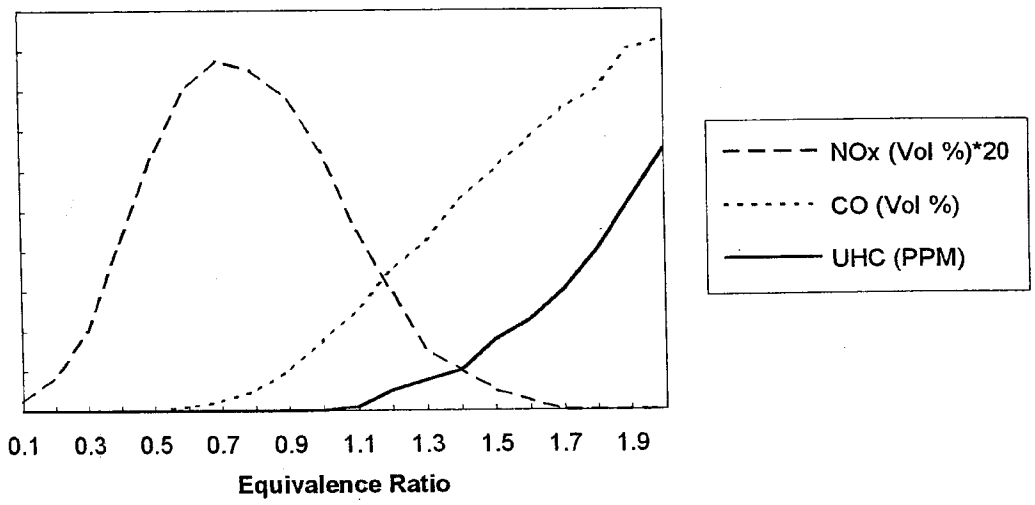

Figure 2.7 – Emissions vs Equivalence Ratio

From this figure, it is clear that the simplest way to reduce NO_X formation in a gas turbine is by operating either rich or lean. Although both

approaches reduce flame temperature and thereby NO_X, each approach (operating either lean or rich) has its disadvantages.

Operating lean will significantly reduce the flame temperature and consequently NO_X emissions. However, fuel lean combustion in the dome region of a gas turbine has stability problems.

Operating rich will reduce NO_X production in three ways. First, thermal NOx formation is decreased by reducing the flame temperature. Second, by operating with a fuel rich mixture, the concentration of available oxygen atoms is reduced. As a result, the production rate of NO decreases. Third, fuel rich combustion provides a large concentration of NO_X consuming HC radicals. However, fuel rich combustion produces excessive amounts of CO and unburned hydrocarbons (UHC). Staged combustion offers the means to utilize the rich burn advantages while avoiding the disadvantages inherent in both rich and lean combustion.

2.4 THE RQL COMBUSTOR CONCEPT

One design for a staged gas turbine combustor is the rich burn - quick mix - lean burn (RQL) combustor (Mosier, et al., 1980). This design, illustrated in Figure 2.8, separates the combustion process into two parts. Within the primary zone, a fraction of the total air reacts with all of the fuel resulting in fuel rich combustion products. This allows for both low flame temperature and high reaction stability. Exiting the primary zone, the combustion emissions react with the remaining air, via dilution jets, in the quick mix region before entering the secondary zone. With the addition of this remaining air, the mixture is converted from fuel rich to fuel lean. As a result, the combustion flame temperature is kept low and the high concentrations of CO and UHC are oxidized.

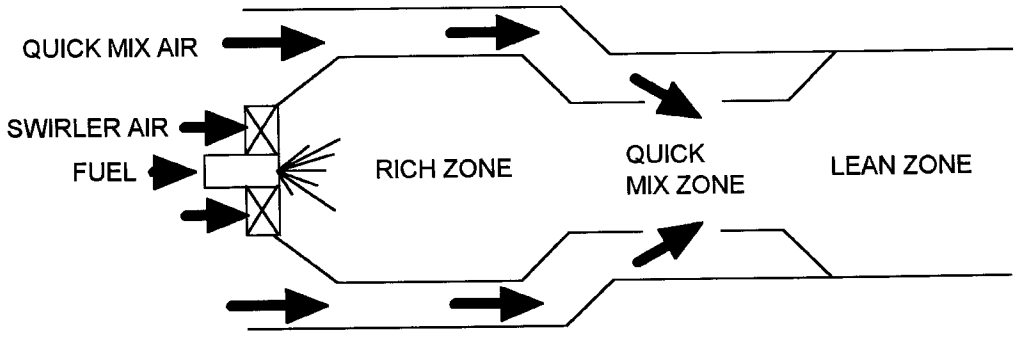

Figure 2.8 - The Rich Burn - Quick Mix - Lean Burn Combustor

2.4.1 PREVIOUS UCI RQL RESEARCH

Brady et al. (1990) studied the operation of the first stage of the RQL, the rich zone. These studies involved the effects of dome geometry on mixing in a rich burn combustor operating at atmospheric conditions without inlet air preheat .

It was concluded from these studies that a significant relationship existed among the rich zone control variables (nozzle air to fuel ratio, reference velocity, swirl strength, inlet geometry and rich zone length) and the degree of mixing. These studies concluded that increases in nozzle fuel to air ratios and reference velocity led to enhanced fuel-air mixing over the range of the experiment. In addition, co-swirling inlet fuel and air streams had superior mixing but reduced stability compared to counter-swirling flows.

2.4.2 ADDITIONAL RQL RESEARCH

The RQL concept, as a means for NOx reduction, has been established for atmospheric cases with and without preheat. In Yamagishi, et al., 1975, an RQL combustor was demonstrated to be successful at reducing thermal and fuel NO at atmospheric conditions with no air preheat Sadakata, et al., in 1981 compared emissions from a two-stage RQL type stationary combustor with those from a single stage combustor. This research also investigated the effects of preheat and determined that NO production increased with increased inlet temperature. Beér, et al., (1982), demonstrated lower NO emissions from a RQL type combustor employing coal liquid fuels.

However, the effects of pressure by itself, and in conjunction with inlet temperature, on NO production from an RQL combustor have yet to be significantly addressed. This study helps to develop an understanding of these effects.

3.0 APPROACH

As mentioned in Section 1.2, the two main goals of this research were to demonstrate the operation of the RQL combustor at realistic operating conditions and to determine the significance of various operating parameters on NO_X emissions and combustion efficiency at realistic conditions. To achieve these goals, the research was divided into three tasks, with each task addressing a separate objective.

1. The first task of the research involved modifying an existing testing facility in order to make it capable of simulating actual gas turbine engine combustor operating conditions. This task of the research is detailed in Section 4.1 of this report.

2. The second task of the research involved the development of a model RQL combustor that would simulate the plenum air feed of real gas turbine engines. This phase of the research is detailed in Section 4.2 of this report.

3. The third task of the research involved the acquisition of emissions data from the model combustor operated at realistic conditions. This task was divided into four parts: experimental development, flow splits tests, Phase 1 emissions testing, and Phase 2 emissions testing. During the experimental development, operating parameters to be examined in relation to NO/NO_X emissions were selected. During the flow splits testing, the plenum feeding of the model RQL combustor was examined and characterized. During the Phase 1 testing the influence of several

operating parameters on NO_X emissions and combustion efficiency would be evaluated. And finally, during the Phase 2 testing, emission profiles would be obtained at the exit of the rich zone and the entrance to the lean zone of the model combustor, while the combustor was operated at realistic conditions. This phase of the research is detailed in section 4.3 of this report.

4.0 EXPERIMENT

4.1 TESTING FACILITY

4.1.1 EXISTING FACILITY

The investigation was conducted in a modified high pressure gas turbine combustor facility at UCI. This facility was originally designed and built to study high pressure fuel spray atomization (Drennan, 1990). In addition, it could incorporate model combustors with optical access that could be probed with laser-based and conventional diagnostics. As originally conceived, this facility could operate at inlet air temperatures and pressures to 920 K and 1700 kPa respectively. The maximum air flow possible was 0.566 m^3/s. The maximum fuel flow was 10 gph, with pressures up to 1500 kPa.

The central component of the test facility was the high pressure vessel housing the model combustor. This vessel, depicted in Figure 4.1, consisted of a plenum air inlet manifold, a vertically traversable nozzle tube, a plenum chamber into which a model can combustor could be mounted, and a water cooled exhaust section.

The vertically traversable nozzle tube was situated on the central axis of this vessel and consisted of a 25.4 mm diameter stainless steel tube housing a 6.4 mm fuel tube. High pressure fuel was supplied through the inner 6.4 mm tube, while fuel atomization air passed through the annulus between the 6.4 mm and 25.4 mm tubes. The inside bottom of the fuel tube was threaded to accommodate a variety of different air assist nozzles. Traversing was accomplished with a stepper motor and electronic control system. The model can combustor was mounted to this nozzle tube, and thus could also be traversed vertically.

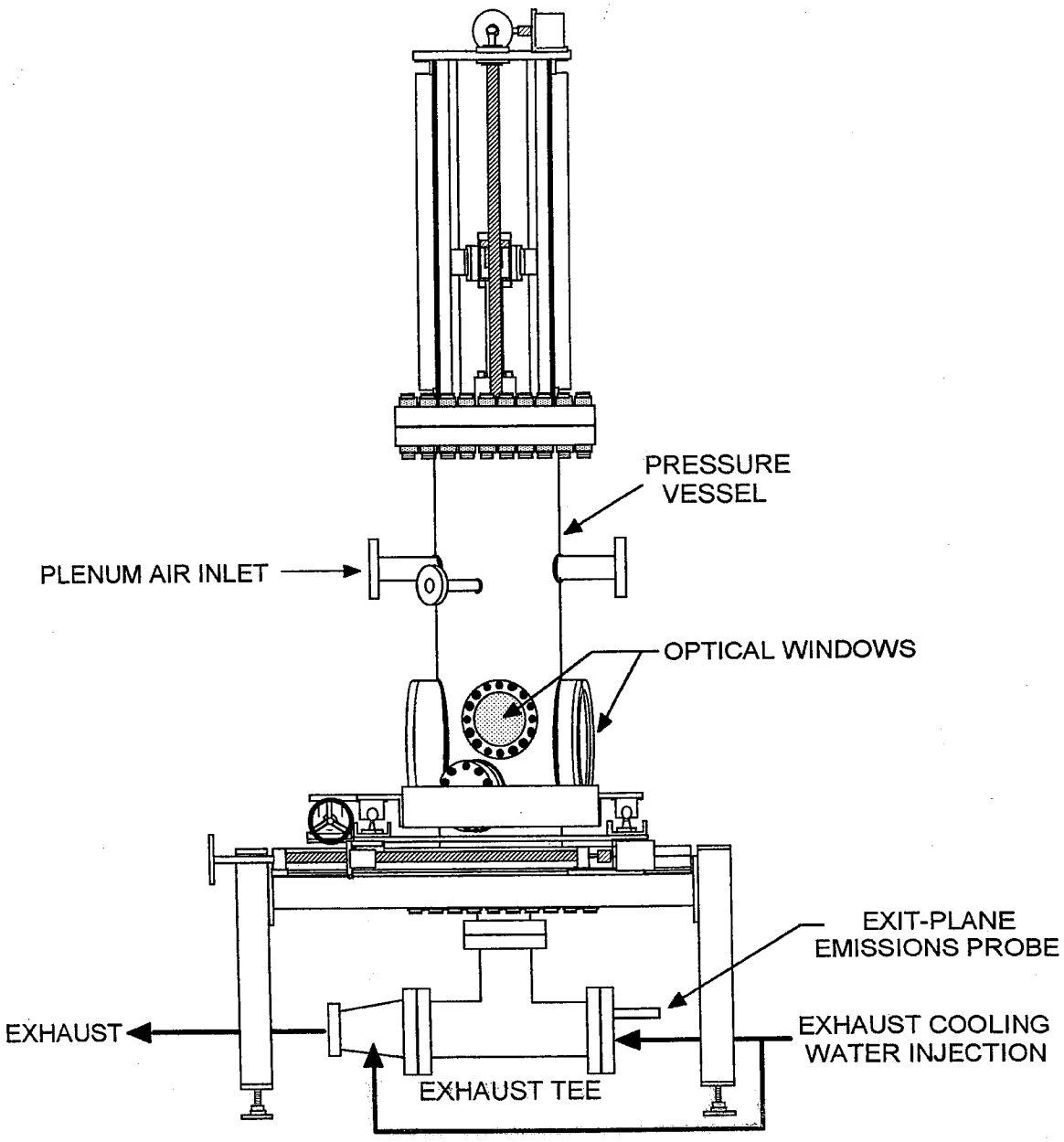

Figure 4.1 – The High Pressure Vessel

The walls of the plenum air inlet manifold and the plenum chamber were fabricated out of 25.4 mm thick chrome-moly steel and were rated to

withstand pressures up to 1722 kPa at temperatures not exceeding 760 K. The inner diameter of the plenum chamber was 38 cm.

Air entering the vessel through the manifold was first directed upward to acheive pressure uniformity and then downward through a flow straightener. This flow straightener consisted of a series of fine stainless steel screens and helped insure a uniform flow into the plenum chamber. A high temperature braided rope seal mounted between the model combustor and the plenum chamber's exhaust seal tube insured minimal air leakage out of the plenum chamber around the combustor. Therefore, once inside the plenum chamber, the air was restricted to exit through the model combustor.

Two doors, mounted 180^{o} apart, allowed for access to the model combustor. In addition, two 17.8 cm diameter, 5 cm thick, fused quartz windows allowed for visual monitoring of the model combustor during tests.

The exhaust section of the vessel, located at the bottom, was cooled through the use of three spatially mounted water spray tubes. A high pressure water pump was utilized to maintain a steady flow of cooling water to the exhaust section.

The air supply system utilized three 300 HP rotary air compressors and a positive displacement booster compressor. Working in parallel, the two standard compressors were capable of supplying 1000 SCFM of air pressurized to 1033 kPa. Working in series with the booster compressor, the compressors could supply 1000 SCFM of air pressurized to 3446 kPa.

After exiting the booster compressor, the air supply was piped into the high pressure facility where it was separated into two flows. The bulk of the air flow was directed into the plenum air line which fed into the high

pressure vessel's plenum chamber. A small portion of the air was directed into a nozzle air line.

The flow rate of air through both air lines was regulated with a pneumatic control valve and a sonic venturi. In both air lines, high pressure air, from the booster compressor, passed through the pneumatic valve and then through the sonic venturis. By choking the flow in the orifices of these venturis, the flow rate of air downstream of the venturis became linearly dependent on the pressure upstream of the venturis. The pressure upstream of the venturies was controlled with the pneumatic valve. For the plenum air supply line, the sonic venturi calibration curve was:

$$\text{Upstream Pressure (psia)} = 0.405 \ (\text{air flow in SCFM}) - 9.80$$

Two different sonic venturis were used for the nozzle air supply line. Each supplied a different range of flows. The smaller of these venturis supplied flow rates between 1 and 15 SCFM. Its calibration was:

$$\text{Upstream Pressure (psia)} = 18.484 \ (\text{air flow in SCFM}) - 5.305$$

The larger of the two venturies allowed for air flows between 10 and 150 SCFM. The calibration for this venturi was:

$$\text{Upstream Pressure (psia)} = 2.101 \ (\text{air flow in SCFM}) - 5.002$$

The pressure within the vessel was controlled with a pneumatic valve located after its exhaust. The pressure in the system was regulated by throttling the exhaust gas flow.

Figure 4.2 illustrates the air supply system.

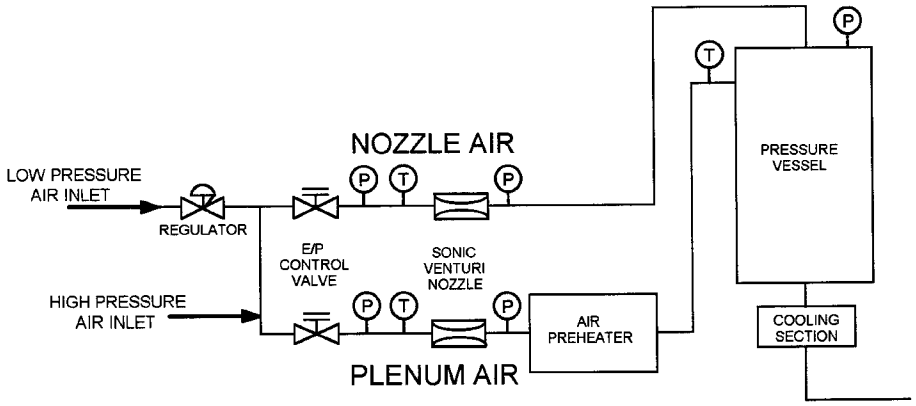

Figure 4.2 - Air Supply System

The fuel supply system utilized a Pulsafeeder pulsating pump to draw fuel from a 13 gallon fuel tank. The flow rate of fuel through the pump could be regulated electronically, and varied from 0 to 10 gph. If the 13 gallon fuel tank was pressurized to 150 kPa with nitrogen, the flow rate through the pump could be increased to 17 gph. The flow rate of the fuel through the pump was also dependent on the pressure downstream of the pump. At higher downstream pressures, lower flow rates were expected. At 1033 kPa downstream, the maximum fuel flow rate was only 6 gph.

The rate of fuel flow to the combustor was regulated through the use of two bypass valves in addition to the fuel coarse and fine feed valves. The fuel system utilized a flow turbine meter, which converted flow rate to Hertz, to determine the flow rate of fuel to the vessel.

4.1.2 MODIFICATIONS

In order to achieve the operating conditions required for this research, several modifications were made to this facility. These modifications involved the addition of (1) increased air preheater capacity, (2) insulation and refractory lining to the air lines and vessel, (3) a high pressure fuel supply system, and (4) an emissions monitoring system.

Heaters. To provide the increased inlet air temperature needed to simulate practical gas turbine engines, it was necessary to provide additional preheat to the plenum air. This heating was accomplished through the use of three electrical resistance heaters working in series. These heaters were built by Watlow and were each capable of heated the air flow to successively higher temperatures. The first of these heaters (previously installed) was capable of heating 1200 SCFM to 700 K. The second heater (new) increased the air temperature to 815 K. The third heater (also new) could increase the temperature to 900 K. The nozzle air supply was not heated prior to entering the high pressure vessel. Since the ratio of nozzle air to plenum air was below 5%, the effects of this deficiency were assumed to be minimal.

Insulation. The plumbing between the heaters and the high pressure vessel was insulated with 5 cm of thick insulating blanket to prevent excessive heat loss. Manufactured by Carborundum, this blanket, called Fiberfrax, consisted primarily of fiberglass. The insulation, rolled around the plumbing, was held in place with a wrapped coil of thin incolel wire. The outer surface of the Fiberfrax was covered with a thin aluminum foil to prevent flaking of the fiberglass.

Insulation was also added to the inner wall of the high pressure vessel. (Figure 4.3) This insulation was a ceramic based refractory, consisting primarily of Al_2O_3, SiO_2, and CaO. Manufactured by Plibrico, this refractory, called Plicast Airlight, had a service limit temperature of 1100 K. The thermal conductivity of this ceramic insulation was 0.65 $btu*in/hr*ft^2*^oF$. By applying a coat 25.4 mm thick to the inner wall of the high pressure vessel, the maximum allowable temperature in the plenum was increased to 1000 K. The addition of this insulation decreased the plenum chamber inner diameter to 31.75 cm.

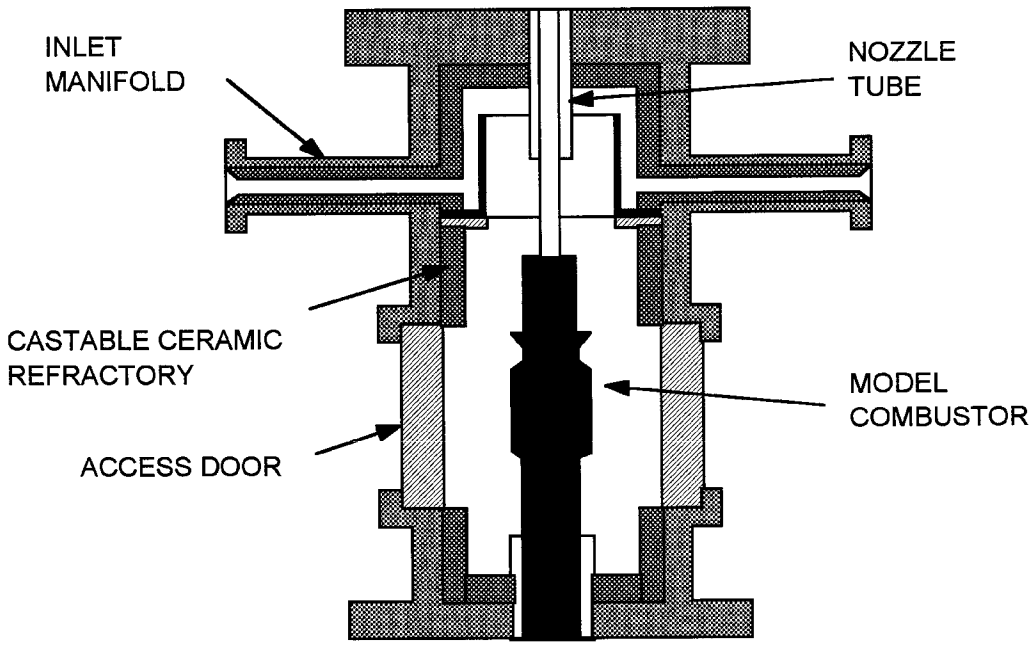

Figure 4.3 - Refractory Coating In High Pressure Vessel

The Plicast Airlight was water based and cast into place. The roof of the high pressure vessel was removed and a round cardboard mold was

inserted into the vessel. The dry refractory was mixed with water and poured into the annular region between the mold and the inner vessel wall. Prior to the pouring, 19 mm steel nails were welded to the inner wall of the vessel. These nails served as anchors for the refractory once it dried. After 48 hours, the cardboard mold was removed and the refractory was thermally treated for 1 hour at 1000 K by passing air through the electrical heaters.

High Pressure Fuel Supply. The added high pressure fuel supply system, depicted in Figure 4.4, utilized a high pressure fuel pump and was supplied with fuel from a 110 gallon fuel tank. This high pressure fuel pump delivered a constant fuel flow rate of 60 gph at a constant pressure of 6900 kPa. This fuel flow rate for this system was also monitored with the turbine flow meter.

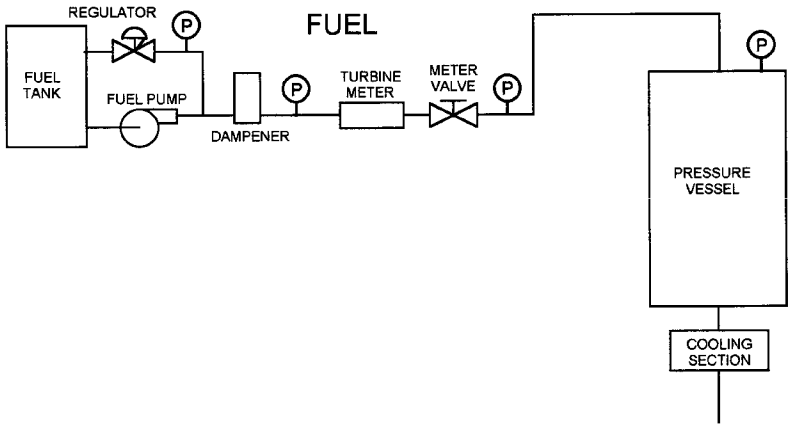

Figure 4.4 - High Pressure Fuel Supply System

Emissions Sampling. During this study, the evolution of the sampling probe design occurred. Initially, only a stationary exhaust plane probe was

used. The stationary water cooled probe is depicted in Figure 4.5. This probe was mounted at the exit plane of the combustor and sampled emissions through three holes. The three holes were arranged to sample the flow from an area weighted distribution as shown in Figure 4.6. In order to minimize reactivity with the sample while maximizing durability, the probe was fabricated out of 316 stainless steel (Grove & Samuelsen, 1984). The emissions measured with this probe were vol% CO_2, ppm CO, vol% O_2, ppm UHC, and ppm NO_x. The stationary probe was located 66 cm downstream of the lean-burn inlet and 84 cm downstream of the nozzle. It was assumed that when the combustion products reached the exit plane probe, equilibrium had been established and the gas temperature was uniform.

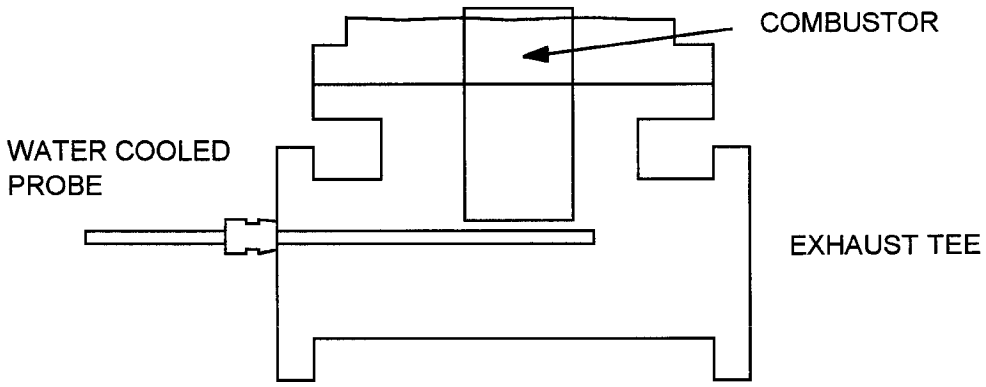

Figure 4.5 - Placement of Stationary Exit Plane Probe

The probe was water cooled to protect the metal from the harsh environment and also to prevent the continuation of the reactions after the sample had entered the probe. The temperature of this cooling water was

maintained above 340 K in order to prevent condensation of water in the combustion products.

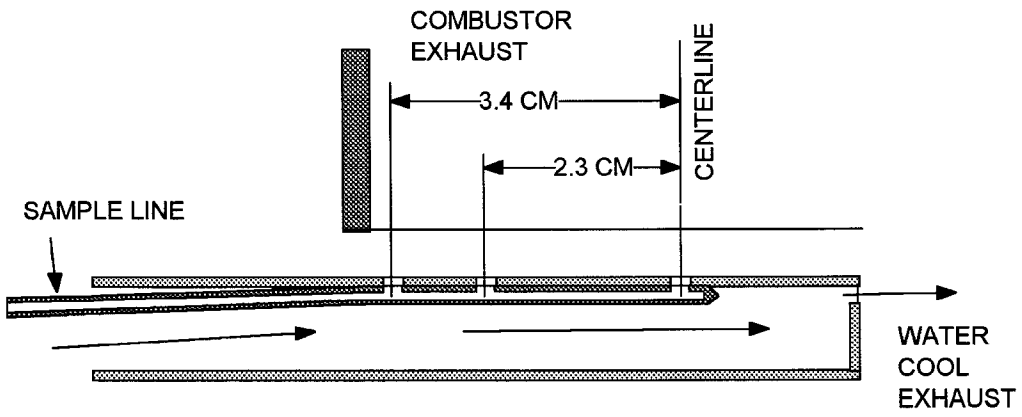

Figure 4.6 - Detail of Stationary Water Cooled Probe Tip

As a part of this study, a second probe was designed and demonstrated that was traversable. It is depicted in Figure 4.7. This probe sampled from a single port and was traversed discrete distances along the radius of the combustor. Through the use of inlet ports mounted to the wall of the model combustor, this probe could sample emissions from the entrance to the lean zone and the exit of the rich zone. Similar to the stationary probe, this probe was fabricated out of 316 stainless steel.

The traversing system for this probe consisted of a traversing table and electronically controlled stepper motor. During testing, the stepper motor was used to move the probe between sampling locations.

The sample lines connecting the probes to the emissions analyzers were maintained at a constant temperature of 400 K with a heated hose. A solenoid valve was used to switch from probe to probe. After the solenoid, the sample passed through three 15 micron filters placed in parallel. These

filters reduced the amount of solids (soot) reaching the analyzers. Following the filters, the sample flow was regulated again with a solenoid, which diverted the flow to either the Emissions Console II (which analyzed CO, O_2, CO_2, NO, and NO_x) or the Hot FID (which analyzed UHC). Figure 4.8 presents the complete sample line.

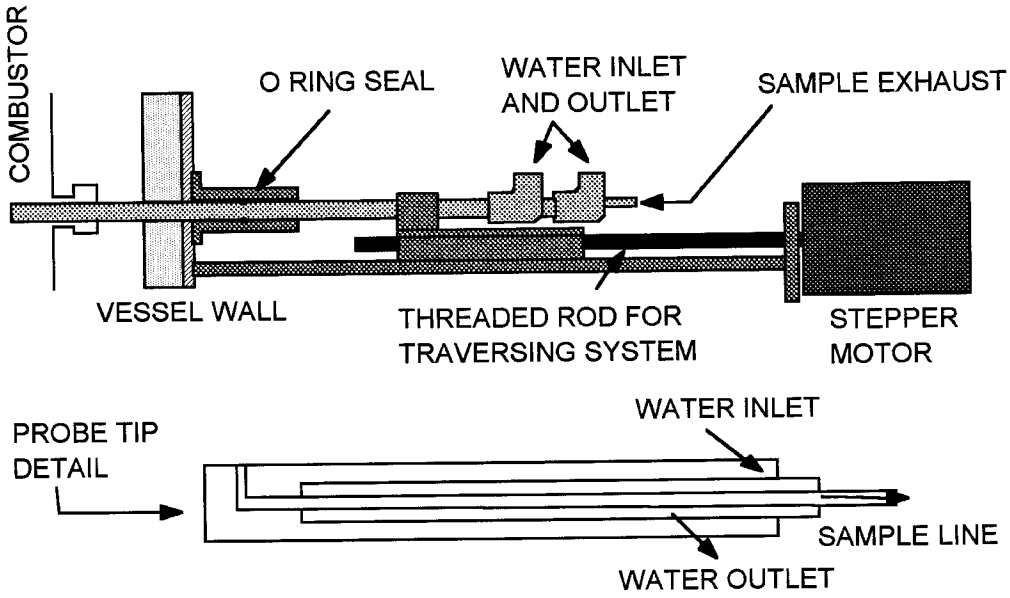

Figure 4.7 - Traversing Probe

The Emissions Console II, presented in Figure 4.9, was built at UCI and consists of a Horiba Model PIR 2000 CO analyzer, a Horiba Model PIR 2000 CO_2 analyzer, a Beckman Model 755 O_2 analyzer, and a Thermo Electron Model 10A Chemiluminescent NO/NO_x analyzer. The sample was drawn into the EC II with a pump and sent through an ice bath which condensed and removed the water. When the combustor was operated under pressure, the sample was pushed through the Emissions Console II without the need of the pump.

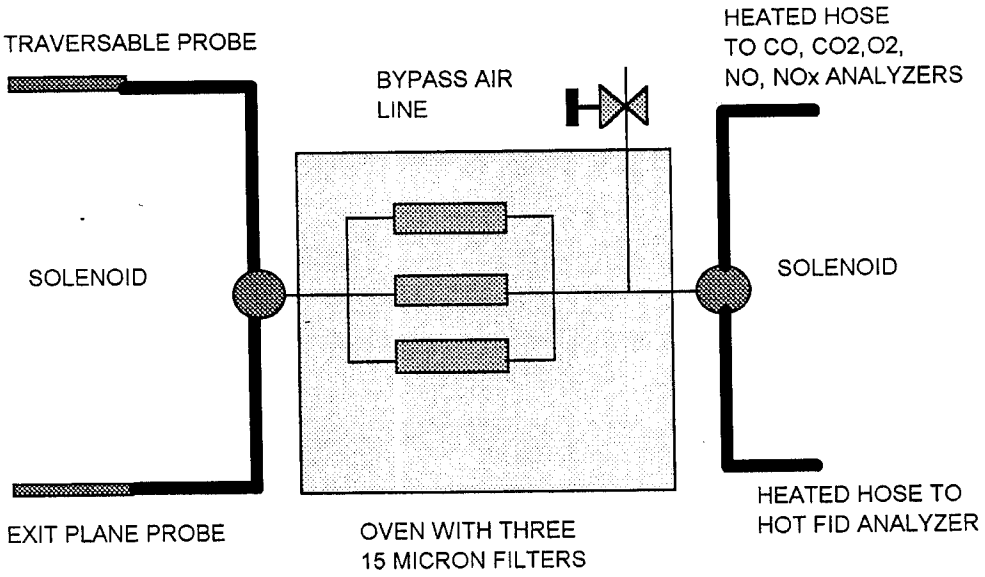

Figure 4.8 - Sample System

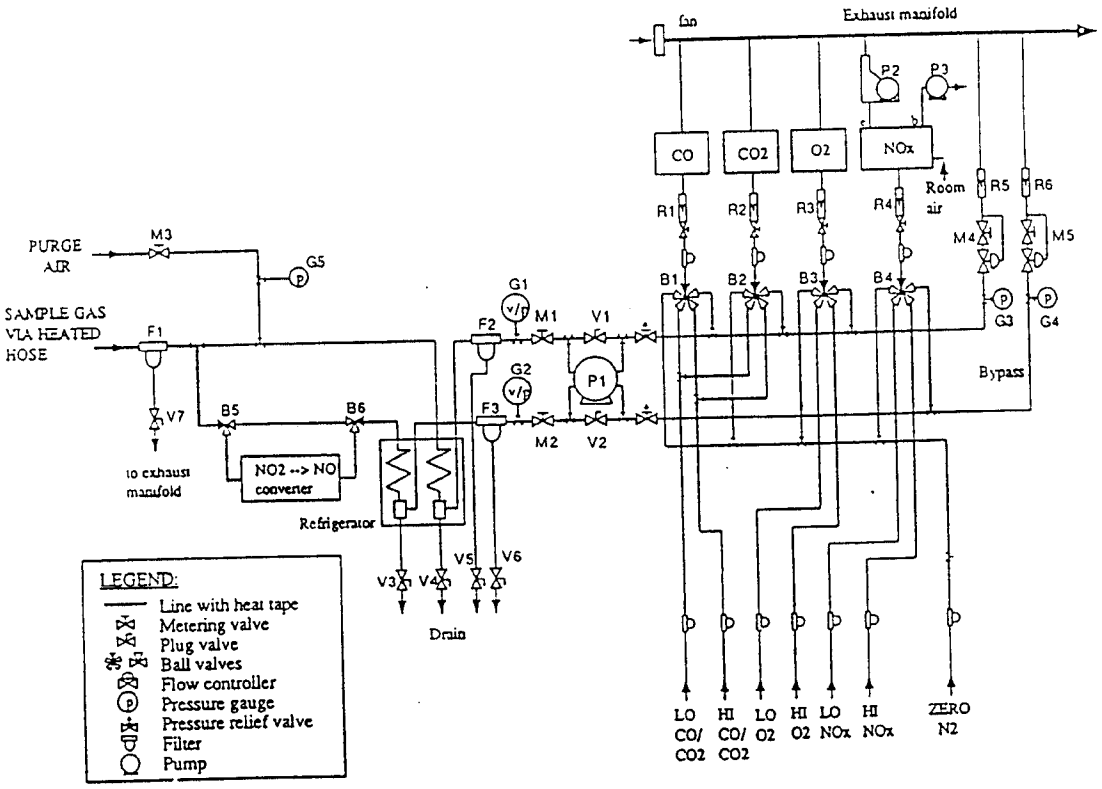

Figure 4.9 - Emissions Console II

Refer to Appendix B for a discussion regarding the operating principles for the analyzers used.

4.2 MODEL RQL COMBUSTOR

Since it was desired to simulate the plenum feeding common to real gas turbine combustors, the model RQL was designed without independently controlled air inlet ports. Air from the plenum entered the combustor through two openings: the aerodynamic swirler or the quick mix dilution jets. As discussed in Section 4.1, the flow splits of air through these openings was predetermined and constant.

Due to the extreme heat of reaction expected during testing (in excess of 2100 K), the combustor was fabricated out of Hastelloy X and the inner walls were lined with a high temperature refractory. Hastelloy X is a nickel-based superalloy with good oxidation resistance at temperatures up to 1500 K and moderately good strength properties up to 1144 K. It has been used in jet engine exhaust nozzles, afterburner components, and structural parts in burner and turbine components. (Mattingly, et al, 1987) The refractory was silica based and could withstand temperatures up to 2255 K.

4.2.1 MODULAR DESIGN

The combustor was modular in design and consisted of five components: the headstock, the rich zone, the quick mix zone, the lean zone and the exhaust section. The modular design enabled varying the geometry of any one combustor part. These five modules were connected with flanges. Figure 4.10 provides a schematic of the fully assembled model RQL.

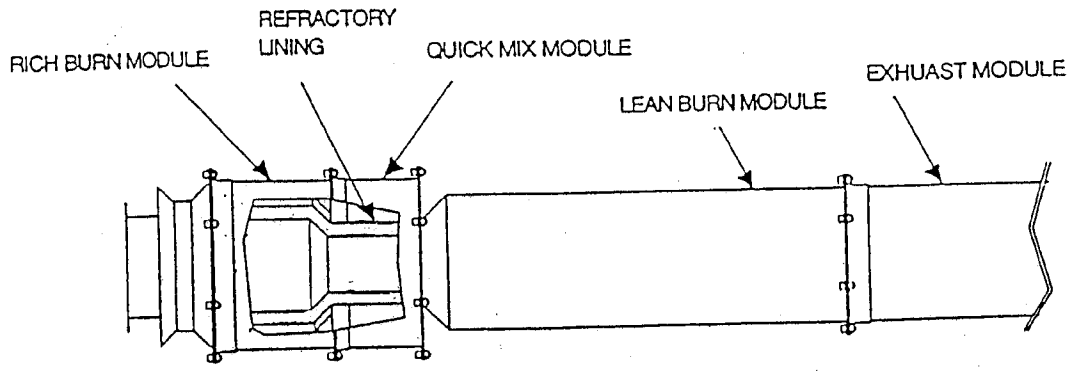

Figure 4.10 – Model RQL – Assembled

The headstock module, depicted in Figure 4.11, connected the model RQL to the high pressure vessel. Fixed to the bottom of the headstock were the aerodynamic swirlers and a quarl which allowed for a 90° expansion. The headstock also housed the ignitor, a combination spark ignitor and hydrogen jet.

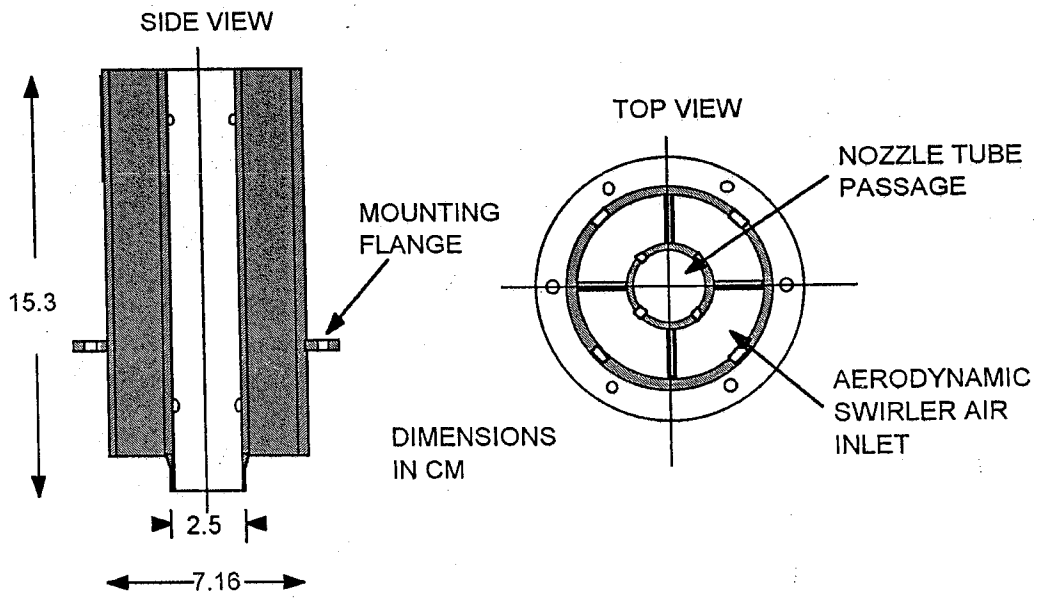

Figure 4.11 - Model RQL - Headstock Assembly

There were two reasons the hydrogen jet ignition system was housed in the headstock module. First, the harsh environment within the dome section would have destroyed the ignitor during each consecutive test. Second, the ignitors presence within the combustor dome section would have resulted in flow disturbances. By placing the hydrogen jet before the aerodynamic swirler, both of these problems were avoided. In addition, by making the ignitor assembly sufficiently small (less than 1 cm in diameter), and by placing it at a sufficient distance behind the swirler (5 cm), negligible disturbance on the symmetry of flow passing through the swirler was insured.

Connected to the bottom of the headstock was the rich zone module, depicted in Figure 4.12.

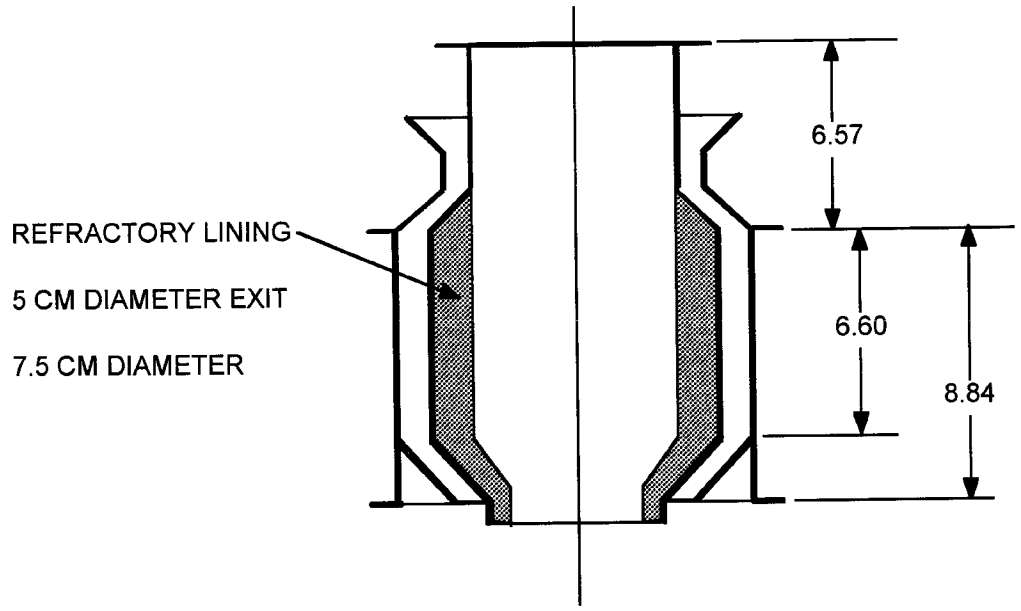

Figure 4.12 - Model RQL - Rich Zone Module

This module was double walled, with fuel rich reaction occuring within the middle section and air flow from the plenum was directed through the inner and outer walls towards the quick mix module's dilution holes. The inner wall of the rich zone module was lined with 1.25 cm of refractory. The inner diameter of the rich zone is 7.6 cm before the contraction and 5.0 cm after. This contraction was located 8.9 cm downstream of the nozzle tip.

Passing through the inner and outer wall of the module before the expansion was a probe inlet port. This port allowed access for the traversing emissions probe. A high temperature braided rope seal provided a relatively air tight seal, while at the same time allowed for the free movement of the probe. The inner diameter of this port was 1.25 cm.

The next module was the quick mix section, depicted in Figure 4.13.

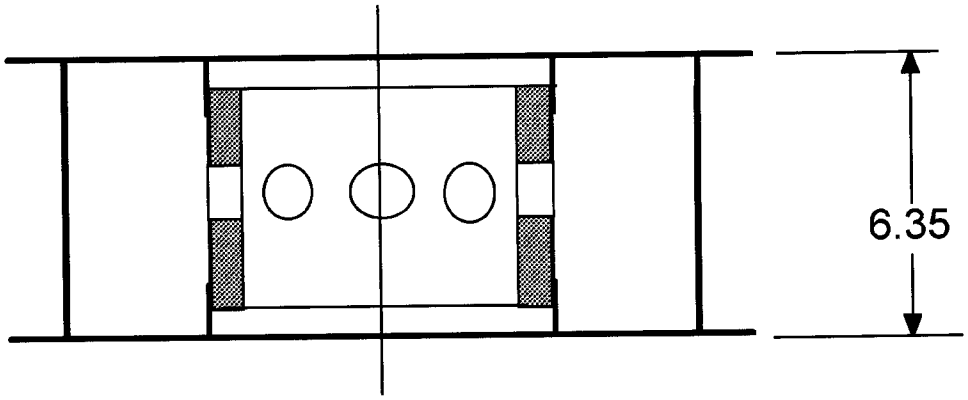

Figure 4.13 - Model RQL - Quick Mix Module

In this module that the remaining plenum air was added to the rich combustion mixture. The inner walls were lined with 1.0 cm of refractory and the inner diameter was 5.0 cm. The total length of the quick mix module was 6.35 cm . There were eight equal area dilution jets. These

jets used a round hole geometry and were 1.25 cm in diameter. It was concluded in a related paper (Hatch, 1991) that the round hole geometry provided the best NO_X control.

Following the quick mix module, was the lean zone and exhaust modules, both of which are depicted in Figure 4.14.

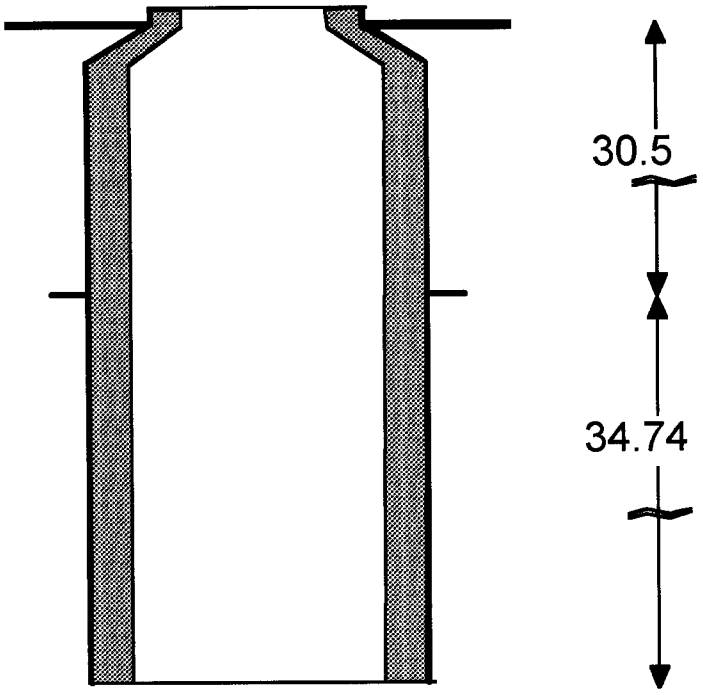

Figure 4.14 - Model RQL - Lean Zone and Exhaust Module

Unlike the rich zone and quick mix, these modules were single walled, with a 1.25 cm layer of refractory lining the walls. The inner diameter of the lean zone was 5.0 cm before the expansion and 7.5 cm after. The diameter of the exhaust module was 7.5 cm throughout the full length. The lean zone was 30.5 cm long, while the exhaust module was 34.74 cm.

Added to the side of the lean zone module was a probe port. Similar to the port in the rich zone, this port allowed access for the traversing emissions sample probe. The axial positions of this port was selected to sample emissions from the quick mix exhaust at a residence time of 3.0 ms for the case where inlet air is 700 K, 800 kPa, and has a reference velocity of 10 m/s.

4.2.2 FUEL ATOMIZER AND FUEL

The model combustor was designed to accommodate a wide variety of fuel atomizers, ranging from practical air blast to research air assist. The atomizer used for this research was a twin fluid, air assist atomizer, which provided a wide fuel flow range and controlled atomization characteristics. This atomizer, depicted in Figure 4.15, was designed and built by Parker Hannifin and produced a high degree of symmetry and reproducibility for inter-laboratory comparison. The primary component of this atomizer was an externally mixing, air assist nozzle, called the Research Simplex Atomizer, or RSA. The fuel exited from a centrally located simplex atomizer tip and mixed with swirling atomizing air. The swirl from this atomizing air ran counter to the swirl generated by the combustor's aerodynamic swirlers. The simplex tip of the RSA was interchangeable to vary liquid flow rate range, droplet diameter, and spray cone angle. The flow rate of fuel through this nozzle was related to the pressure drop across it by the following equation:

FN = (fuel flow in lbs/hr) / sqrt(pressure drop across nozzle in psid)

where FN was the flow number corresponding to the particular nozzle. For this research the RSA nozzle had a flow number of 4.57. During operation, this number was checked by measurements made of both the fuel flow and the pressure drop across across the nozzle.

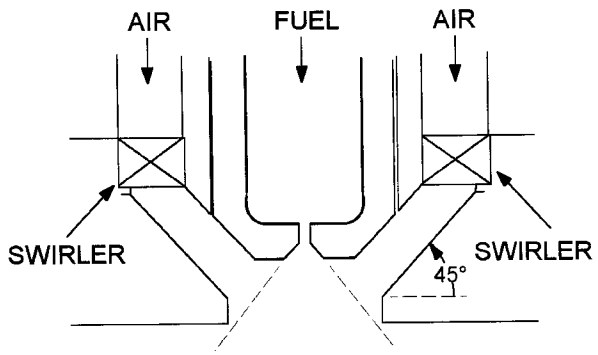

Figure 4.15 - Fuel Atomizer

This nozzle design produced nominally 10 micron SMD droplets as measured by the laser diffraction technique at a fuel pressure drop of 687 kPa (100 psid). While the RSA was not a production industrial gas turbine atomizer, the atomizer displayed many of the features of practical gas turbine atomizers such as a pressure atomizing simplex tip and air injection to aid in the formation of a fine fuel spray.

The fuel used for this research was Jet-A. Jet-A is represented by the formula $C_{12}H_{23}$. The specific gravity for Jet-A is 0.813. (Martel, 1988)

4.2.3 SWIRLERS

Swirl was generated from one of two flat vaned swirlers, each of which had vane angles of 60^{o}. The two swirlers had two different effective areas.

Using the larger swirler, a 3:1 flow split was achieved. A 4:1 flow split was achieved with the smaller swirler.

4.3 EXPERIMENTAL DESIGN AND EXECUTION

4.3.1 EXPERIMENTAL DEVELOPMENT

Five combustor operating parameters important to NO/NO_X production and combustion efficiency are operating pressure, inlet air temperature, reference velocity, lean zone equivalence ratio and overall equivalence ratio.

The significance of inlet temperature lies in its direct proportionality to flame temperature. Since thermal NO_X production is exponentially dependent on flame temperature it can be exponentially linked to inlet temperature as well.

Operating pressure has been shown to be significant in both thermal NOx production and prompt NO_X production (Heberling, 1976). Pressure has also been shown to have an influence on CO and UHC emissions with CO and UHC concentrations decreasing at higher pressures. (Lefebvre, 1983)

Reference velocity is inversely proportional to reaction residence time which is significant in both thermal NOx production and CO oxidation. Previous studies have demonstrated that combustor residence time can be linked to thermal NO emissions by the following expression:

$$\ln\left[EI(NO)/t\right] = -72.28 + (2.80)\left[\mathrm{sqrt}(T)\right] - T/38$$

where T is the flame temperature in Kelvin and t is the residence time in seconds (Lefebvre, 1983). The effect of residence time on thermal NO

formation has been shown (Anderson, 1975) to be less significant at lower equivalence ratios ($\Phi < 0.4$).

The rich zone equivalence ratio is significant in its relationship to rich zone reaction temperature and the concentration of rich zone HC radicals. It defines the inlet composition to the quick mix region which has the greatest impact on the NO_X production.

The lean zone equivalence ratio is significant in its relationship to lean zone flame temperature and the oxidation of input CO.

The rich zone and lean zone equivalence ratios are also important to NO_X production in that they dictate the relative significance of the transition between the two zones, in the quick mix region. In order to maintain low NO_X, it is necessary to pass the fuel rich products rapidly through the stoichiometric state to reach the fuel lean region. However, the transition time must be significant enough for oxidation of CO and UHC to occur. The smaller the ratio of rich zone to lean zone equivalence ratio, the greater the extent to which stoichiometric regions can form within the transition region in the quick mix dilution jets and consequently, the greater the residence time within this transition region.

4.3.2 FLOW SPLIT TESTING

Since the model combustor was designed to operate with plenum feeding, it was necessary to determine quantitatively the ratio of plenum air entering the combustor through the aerodynamic swirler to that entering through the quick mix dilution jets. In order to quantify this ratio, a series of flow split tests were conducted.

The flow split tests consisted of three phases. During the first phase, the combustor was placed in the high pressure vessel and the air inlets to both

the swirler and the dilution jets were sealed. Plenum air was then added to the plenum chamber. With both combustor inlets plugged, the only means of exhaust for the plenum air was through the seal tube rope seal. By measuring the flow rate of air into the vessel relative to the pressure differential across the rope seal, a calibration curve was established relating the rate of leakage across the seal to the pressure differential across the combustor.

During the second phase of the flow splits test, the inlet to the aerodynamic swirlers was opened but the inlet to the dilution jets was left closed. Plenum air was again added to the plenum chamber and a calibration curve was established relating flow rate into the plenum chamber to the pressure drop across the combustor. Since the leakage through the rope seal was known for a given pressure drop, it was possible to establish a relation between the flow rate of plenum air through the swirlers to the pressure drop across the combustor. This relation indicated that for flow rates above 80 SCFM, the pressure drop across the combustor increased linearly with the flow rate of plenum air through the swirlers.

For the third phase of the flow split tests, both the inlets to the model combustor were opened and air was added to the plenum. Another calibration curve was established relating the flow into the plenum chamber to the pressure drop across the combustor. Since the rate of leakage through the rope seal and the rate of air passage through the swirlers was known for a given pressure drop, it was possible to compute the flow rate of air through the dilution jets for a given pressure drop. From this curve, similar to that established for the swirler, it was established that for flow rates above 60 SCFM, the pressure drop across the combustor increased linearly with flow rate through the dilution jets.

Combining the results from the three phases of the flow split tests, the ratio of flow passing through the swirlers to that passing through the dilution jets was computed. Since above 80 SCFM, the pressure drop across the combustor was linearly related to the flow rate of air flow through the two inlet ports, it was assumed that this computed flow split ratio was constant for all flow cases above 80 SCFM.

By performing these series of tests twice, each time with a different size aerodynamic swirler, two different flow splits were established. With the smaller swirler, a flow split of 4:1 was computed. In other words, for air flow rates into the plenum above 80 SCFM, 20% of the plenum air entered the combustor through the swirlers while the remaining 80% entered through the dilution jets. From these tests it was concluded that, for the air flow rates tested, the air leakage through the rope seal was negligible. With the larger swirlers, the flow split was computed to be 3:1. Thus, 25% of the plenum air entered through the swirlers while 75% entered through the dilution jets.

4.3.3 PHASE 1 TESTING: PERFORMANCE ASSESSMENT

During the Phase 1 tests, exit plane emissions data were obtained for the model RQL combustor as it was operated under a number of different conditions. The five operating conditions varied were inlet temperature to the combustor, pressure, plenum air reference velocity, rich zone equivalence ratio, and lean zone equivalence ratio. The pressure measured was that of the plenum air before entering the model combustor. The reference velocity variable was a theoretical value approximating the velocity of the plenum air passing through the combustor lean zone at the plenum chamber temperature and pressure.

Two sets of equivalence ratios were chosen for each of the flow split studies. For the 4:1 flow split, the combustor was first operated with rich zone and lean zone equivalence ratios of 1.5 and 0.3, and second with rich zone and lean zone equivalence ratios of 2.0 and 0.4. For the 3:1 flow splits, the combustor was first operated at rich zone and lean zone equivalence ratios of 1.5 and 0.375, and second at 2.0 and 0.5. By keeping the rich zone equivalence ratio between 1.5 and 2.0, relatively low reaction temperature and soot formation could be maintained. The lean zone equivalence ratio was varied between 0.5 and 0.3 to maintain a relatively cool exhaust temperature.

For each set of equivalence ratios, the model combustor was tested at three different plenum air reference velocities (10 m/s, 15 m/s, and 20 m/s), four different inlet temperatures (367 K, 533 K, 700 K, and 867 K), and various pressures between 200 kPa and 1033 kPa atm. 367 K was chosen as the inlet lowest temperature in order to prevent saturation of the refractory walls by liquid fuel injected prior to ignition. 200 kPa was chosen as the lowest pressure setting in order to maintain a stable flame. During initial test runs of the model RQL combustor, it was noted that it was difficult to maintain a stable flame under atmospheric conditions.

For all tests, the air/liquid ratio in the nozzle was kept constant at 1.0. In total, 122 different test cases were investigated. The test conditions selected were chosen to provide an emissions database for a broad range of operation and were dependent on the availability of plenum air (required less than 1000 SCFM). Data Tables 4.1 through 4.4 list the different test cases which made up the Phase 1 test matrix.

	200 kPa	300 kPa	400 kPa	500 kPa	600 kPa	700 kPa	800 kPa	900 kPa	1000 kPa
367 K		10, 20 m/s	10,15, 20 m/s	15 m/s	10 m/s	10 m/s			
533 K	10, 15 m/s		10, 15, 20 m/s	20 m/s		10, 15 m/s			10 m/s
700 K	15,20 m/s		10,15 m/s			10,15, 20 m/s			10 m/s
867 K	15, 20 m/s		15,20 m/s			15,20 m/s		15 m/s	

Date Table 4.1 - 0.3 Lean Zone Φ, 1.5 Rich Zone Φ

	200 kPa	300 kPa	400 kPa	500 kPa	600 kPa	700 kPa	800 kPa	900 kPa	1000 kPa
367 K	10, 20 m/s	10,15, 20 m/s	10,15, m/s	15 m/s		10 m/s			
533 K	10, 15, 20 m/s	10 m/s	10, 15, 20 m/s	20 m/s		10, 15 m/s			
700 K	10,15, 20 m/s		10,15 20 m/s		10,15, 20 m/s	10,15, m/s		15, 20 m/s	10 m/s
867 K									

Date Table 4.2 - 0.375 Lean Zone Φ, 1.5 Rich Zone Φ

	200 kPa	300 kPa	400 kPa	500 kPa	600 kPa	700 kPa	800 kPa	900 kPa	1000 kPa
367 K	10, 20 m/s	10, 15 m/s	15, 20 m/s			10,20 m/s			20 m/s
533 K	10, 15 20 m/s		10, 15, 20 m/s	20 m/s	15 m/s	10, 15 m/s			10 m/s
700 K	10,15, 20 m/s		10,15 20 m/s		20 m/s	10,15, m/s			10 m/s
867 K	15, 20 m/s		15,20 m/s			15,20 m/s		15 m/s	

Data Table 4.3 - 0.4 Lean Zone Φ, 2.0 Rich Zone Φ

	200 kPa	300 kPa	400 kPa	500 kPa	600 kPa	700 kPa	800 kPa	900 kPa	1000 kPa
367 K	10 m/s	10 m/s		10 m/s					
533 K	10, 15 20 m/s	20 m/s	15,20 m/s	10,15 m/s		10 m/s			
700 K	15 m/s	20 m/s	10,15 20 m/s			10,15, m/s			10 m/s
867 K									

Data Table 4.4 - 0.5 Lean Zone Φ, 2.0 Rich Zone Φ

4.3.4 PHASE 2 TESTING: DETAILED MEASUREMENTS

The Phase 2 tests involved obtaining emissions profiles at the exit of the rich zone and the entrance to the lean zone. For these tests, the combustor was operated at the following conditions: T3 = 700 K, P3 = 400 kPa, Ref Vel = 10 m/s, Overall Equivalence Ratio = 0.375, and Rich Zone Equivalence Ratio = 1.5. Since these tests seeked to establish the relative contribution of the rich zone and lean zone to the overall production of NO_x, the operating pressure, temperature and reference velocity were chosen at random. The lean zone and rich zone equivalence ratios were chosen to represent average conditions.

The traversable water cooled probe was used to obtain emissions (NO, NO_x, O_2, CO, CO_2 and UHC) at six radial positions in the rich zone exit and eleven radial positions in the lean zone entrance. (Figure 4.16)

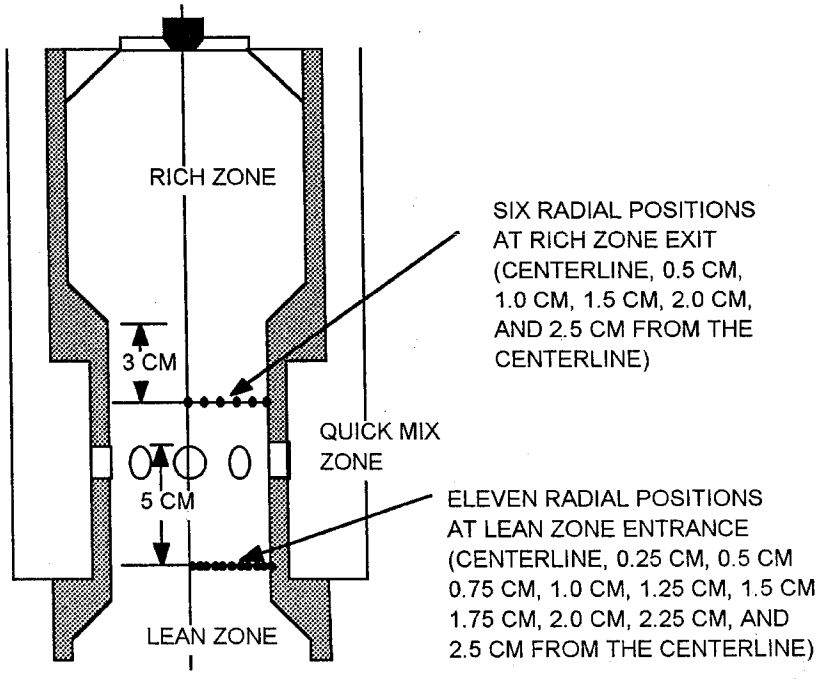

Figure 4.16 – Phase 2 Testing Locations

For this research, the start of the lean zone was designated by the leading edge of the round holes of the quick mix dilution jets. The combustor was assumed to be axisymmetric. As a result, emissions data were obtained for only half of the combustor.

5.0 RESULTS

5.1 PHASE 1 TESTING

5.1.1 NO_X EMISSIONS

The measure of NO_X in the combustor exhaust was evaluated with a computed Emission's Index ($EI(NO_X)$). This index value indicated the ratio of grams of NO_X present in the exhaust to the kilograms of fuel consumed.

The emissions of NO_X, measured in ppm, were converted to the NO_X Emission Index with the following formula (derived in Appendix A):

$$EI(NO_X) = [MW_{NO_2}/MW_{dry\ exhaust}]\ [(100 - \%H20)/100]$$
$$[\text{mass flow rate of exhaust in grams/fuel flow rate in kg}]\ NO_X\ ppm$$

Rich Zone $\Phi = 1.5$, Lean Zone $\Phi = 0.3$. The first series of Phase 1 tests involved operating the model RQL combustor with a rich zone equivalence ratio of 1.5 and a lean zone equivalence ratio of 0.3. The combustor was operated at three different air reference velocities (10 m/s, 15 m/s, and 20 m/s). For the 10 m/s reference velocity case, the combustor was run at three inlet temperatures (367 K, 533 K, and 700 K). An additional inlet temperature of 867 K was added to the 15 m/s and 20 m/s cases. The computed $EI(NO_X)$ values for these test cases are presented in Figures 5.1 through 5.3.

Comparisons of the cases where inlet temperature and reference velocity are held constant while pressure is increased reveal a tendency between increased NO_X production and increased pressure. With a few exceptions, this relation tends to appear more pronounced at lower pressures. For example, for the 10 m/s, 533 K test cases in Figure 5.1 (black circles) the

$EI(NO_X)$ value climbs steadily between 2 and 6 atmospheres. However, there is little addition when pressure is further increased to 10 atmospheres.

Among the execptions to this trend are the cases involving higher inlet air temperatures and lower reference velocities. When the combustor is operated with 700 K inlet temperature and a 10 m/s reference velocity, a near linear relation between $EI(NO_X)$ and operating pressure appears over the range of 4 to 10 atmospheres (white triangles) When the reference velocity is increased to 15 m/s, with inlet temperature being held constant at 700 K, the $EI(NO_X)$ no longer increases steadily with pressure (Figure 5.2). Here, the $EI(NO_X)$ appears to level out for pressures greater than 6 atmospheres. However, when the inlet temperature is increased to 867 K, the near linear relation between $EI(NO_X)$ and pressure appears again (black triangles). Increasing the reference velocity to 20 m/s appears to eliminate this near linear relationship (Figure 5.3).

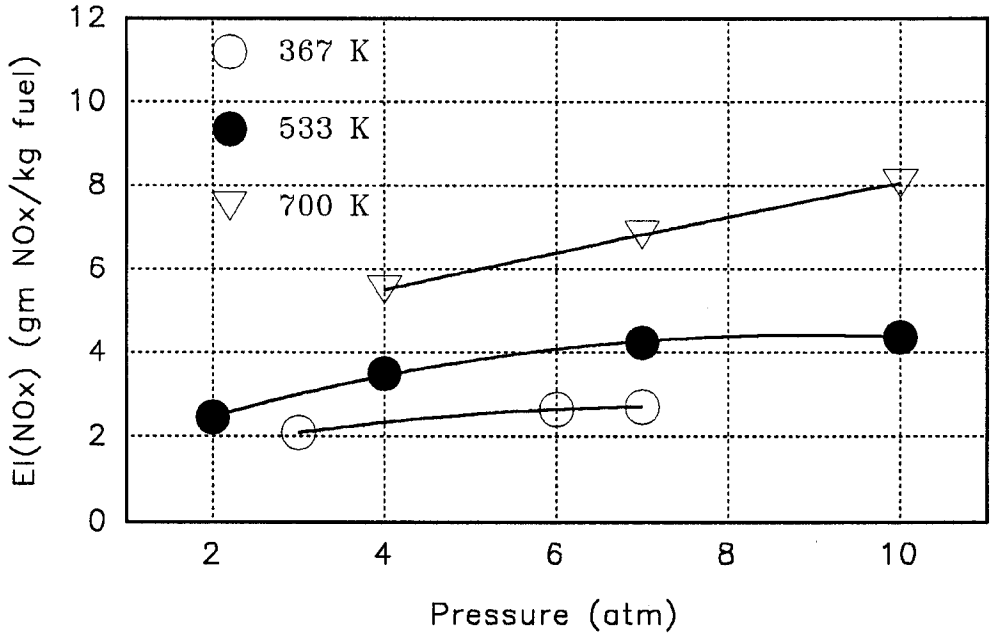

Figure 5.1 - $EI(NO_X)$ for RZ $\Phi = 1.5$, LZ $\Phi = 0.3$, Ref Vel = 10 m/s

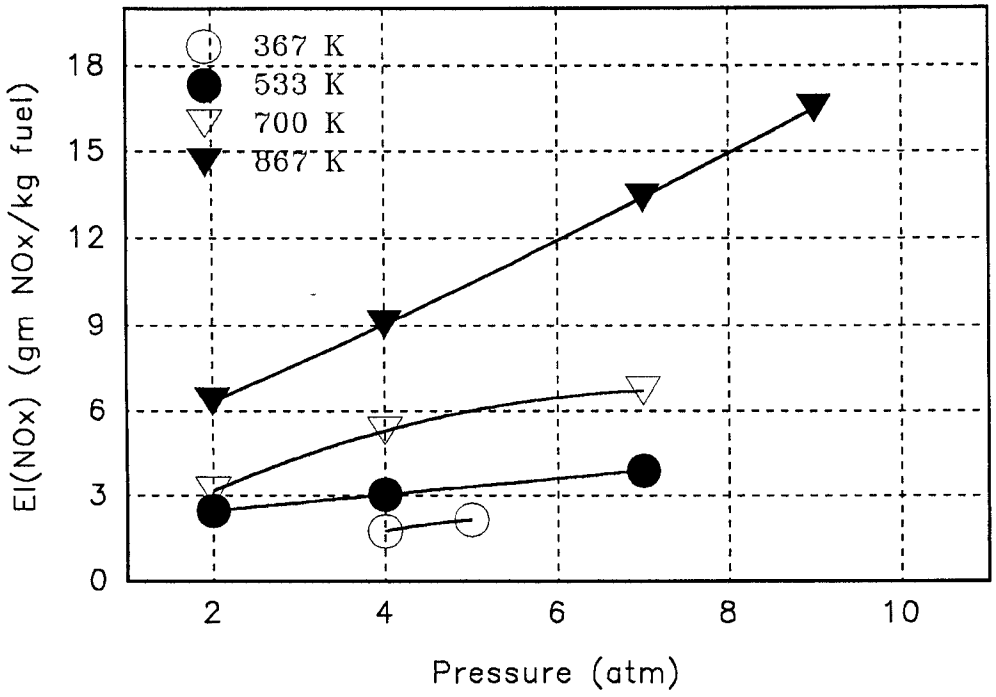

Figure 5.2 - EI(NO_X) for RZ Φ = 1.5, LZ Φ = 0.3, Ref Vel = 15 m/s

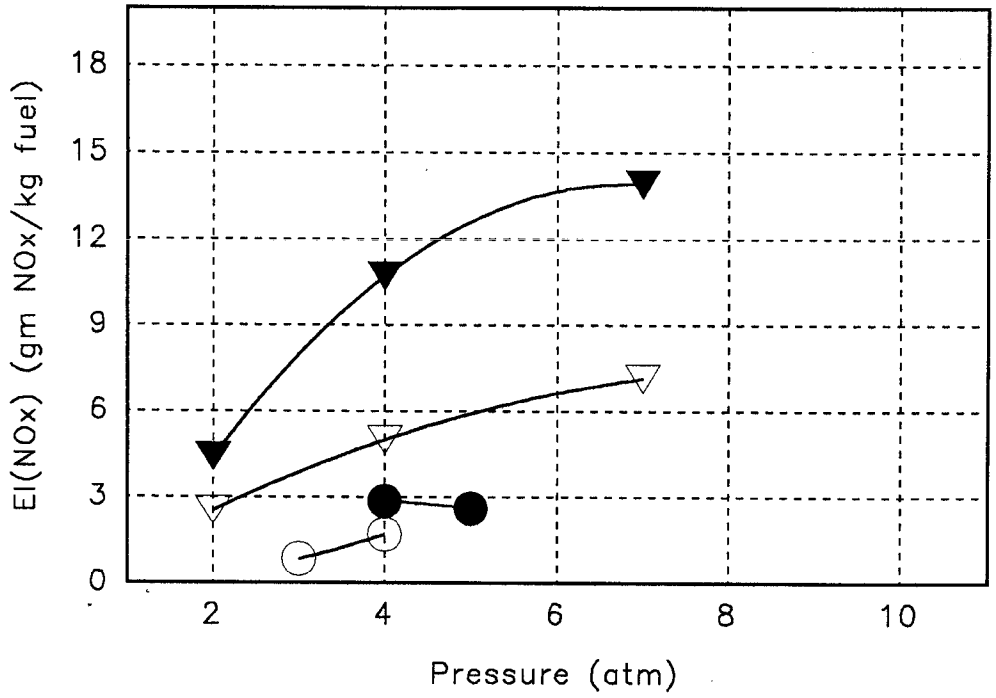

Figure 5.3 - EI(NO_X) for RZ Φ = 1.5, LZ Φ = 0.3, Ref Vel = 20 m/s

Past studies (Allen, 1976; Lipfert, 1976; Donovan et al., 1978; Fowler et al., 1993) have shown that $EI(NO_X)$ production can be related to inlet pressure by the following equation:

$$EI(NO_X) \alpha P^n$$

where n can vary from 0.5 to 0.75. The physical reason behind this correlation is not entirely understood. However, much of it can be attributed to the relationship between increased reaction temperature resulting from increased pressure.

Regression analysis of these data (Refer to Appendix C), however, showed that for this staged combustor, the $EI(NO_X)$ varied proportionally with combustion pressure to the 0.4 power:

$$EI(NO_X) \alpha P^{0.4}$$

Figures 5.1 through 5.3 also illustrate the effect of increases in inlet temperature on NO_X production for the 0.3, 1.5 cases. As expected, constant incremental increases in inlet temperature result in continuously larger increases in NO_X production. For example, in the case where pressure and reference velocity are held constant at 4 atmospheres and 15 m/s (Figure 5.2) , the $EI(NO_X)$ increases from 1.76 to 3.04 to 5.3 to 9.05 as inlet temperature is raised from 367 K to 533 K to 700 K to 867 K. This trend supports the exponential relation between reaction temperature and the rate of NO_X formation described by Zeldovich.

The effect of reference velocity is not quite as pronounced as that of either temperature or pressure. Generally, there is a noticeable drop in the

$EI(NO_X)$ as reference velocity increases. For example, with inlet temperature and operating pressure held constant at 700 K and 2 atmospheres, an increase in reference velocity from 15 m/s to 20 m/s coincides with a slight decrease in $EI(NO_X)$ from 3.12 to 2.45. A significant factor leading to this drop is the resulting decrease in residence time due to the increased flow velocity. In passing from the rich zone to the lean zone, the combustion products must pass through region of stoichiometry. Within this region, reaction temperature reaches a maximum as does NO_X production. A decrease in reference velocity results in an increase in residence time for the combustion products within this region.

Rich Zone Φ = 1.5, Lean Zone Φ = 0.375. Figures 5.4 through 5.6 present the results obtained from the cases where the lean zone equivalence ratio was raised to 0.375, while the rich zone equivalence ratio was held constant at 1.5.

This increase in lean zone equivalence ratio (Φ_{lz}) results in a general increase of the $EI(NO_X)$ by 20%. For example, in Figure 5.4, an EI(NOx) value of 8.9 results from operation of the model combustor when the inlet temperature, pressure and reference velocity are 700 K, 7 atmospheres, and 10 m/s respectively (Figure 5.4). This is a 25% increase in EI(NOx) for the model RQL operating at the same conditions with a lean zone equivalence ratio of 0.3 (Figure 5.1).

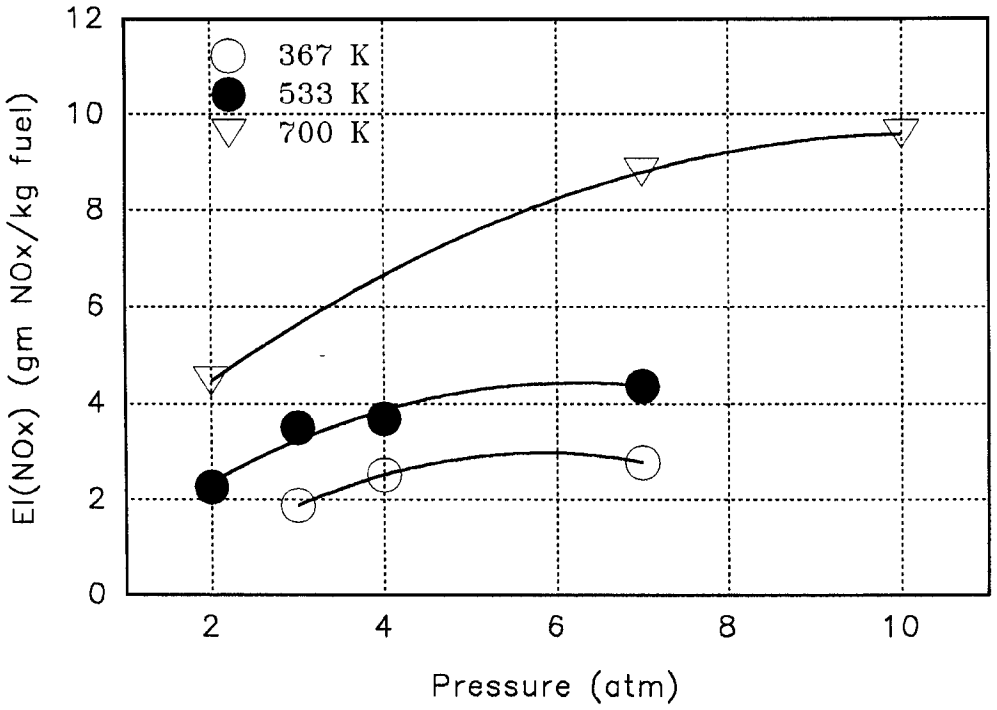

Figure 5.4 - EI(NO_X) for RZ Φ = 1.5, LZ Φ = 0.375, Ref Vel = 10 m/s

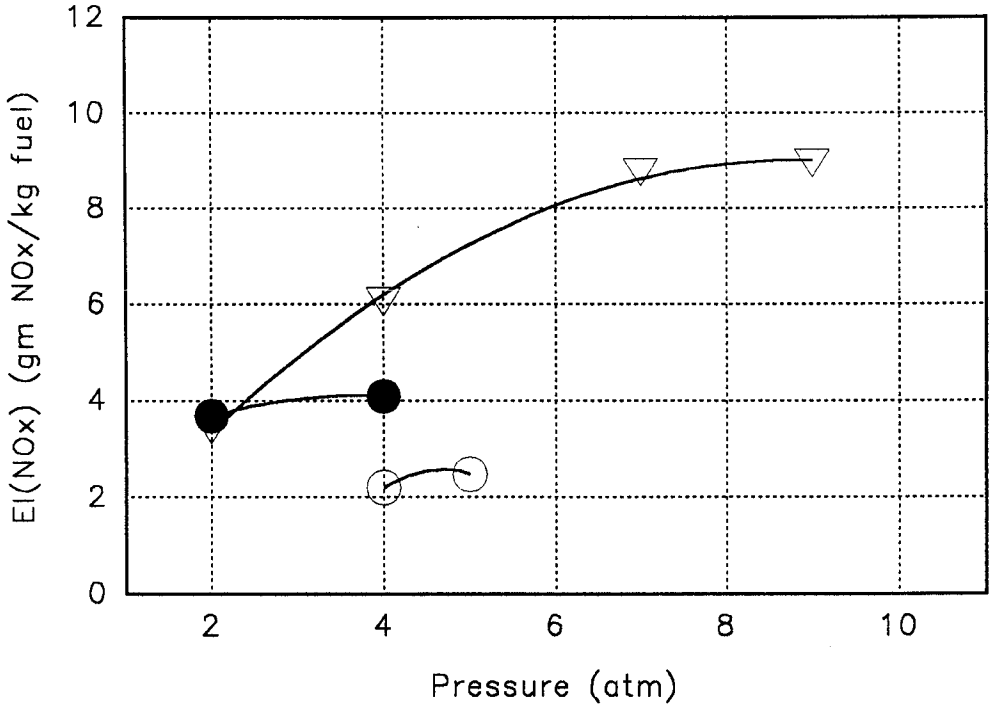

Figure 5.5 - EI(NOx) for RZ Φ = 1.5, LZ Φ = 0.375, Ref Vel = 15 m/s

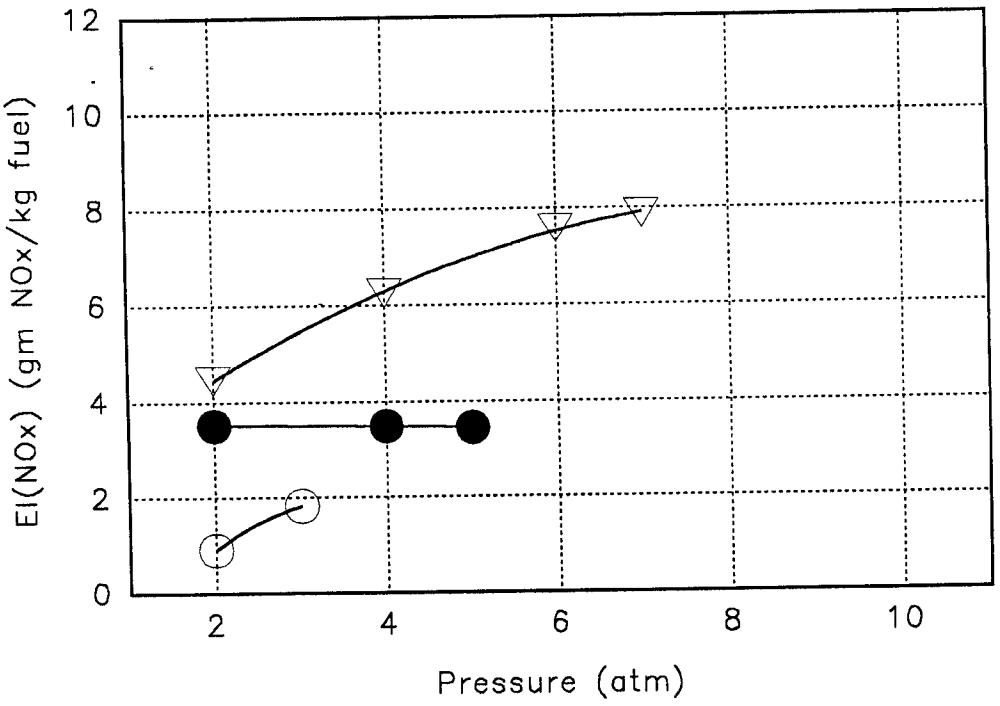

Figure 5.6 - EI(NO_X) for RZ Φ = 1.5, LZ Φ = 0.375, Ref Vel = 20 m/s

Such an increase can, in part, be attributed to the dependence of flame temperature on equivalence ratio. However, for this particular combustor, the effect of changes in the momentum flux out of the quick mix region must also be considered. In order to vary the lean zone equivalence ratio from 0.3 to 0.375 while holding the rich zone equivalence ratio constant, it is necessary to increase the relative amount of total mass put through the combustor's rich zone from 21.6% to 26.9% and decrease the relative amount of total mass added through the air addition stage jets from 78.4% of the combustors total mass to 73.1%. This results in a substantial decrease in the momentum flux of the flow entering the combustor through the quick mix dilution holes. Such a decrease in the momentum flux could

result in substantially lower air jet penetration and degraded mixing with its resultant increase in NO_X production.

For this set of equivalence ratios, the same general trends are found regarding pressure, inlet temperature and reference velocity. $EI(NO_X)$ increases to a fractional power with increased pressure and temperature and decreases with increased reference velocity.

Rich Zone $\Phi = 2.0$, Lean Zone $\Phi = 0.4$. Figures 5.7 through 5.9 present the computed $EI(NO_X)$ values for the cases where the rich zone equivalence ratio was increased to 2.0 and the lean zone equivalence ratio was increased to 0.4.

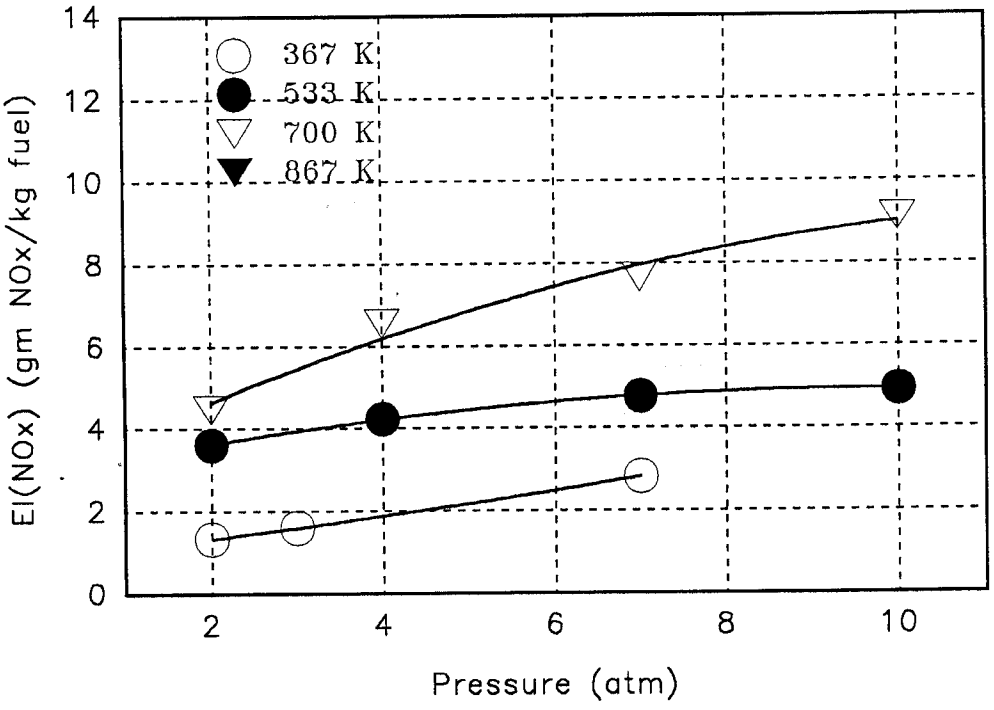

Figure 5.7 - $EI(NO_X)$ for RZ $\Phi = 2.0$, LZ $\Phi = 0.4$, Ref Vel = 10 m/s

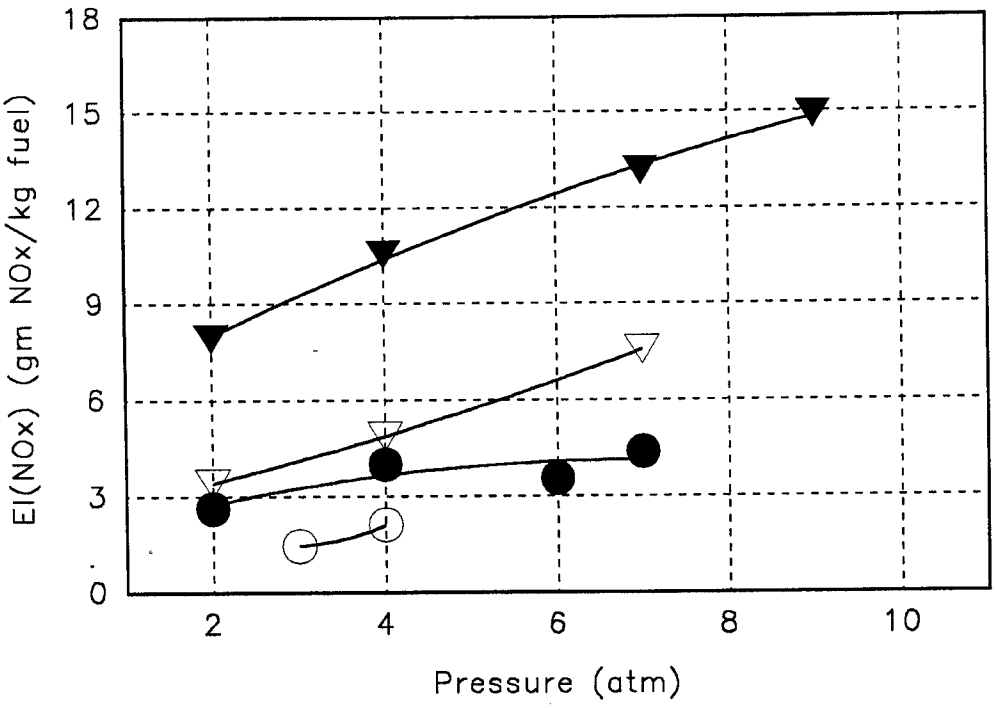

Figure 5.8 - EI(NO_X) for RZ Φ = 2.0, LZ Φ = 0.4, Ref Vel = 15 m/s

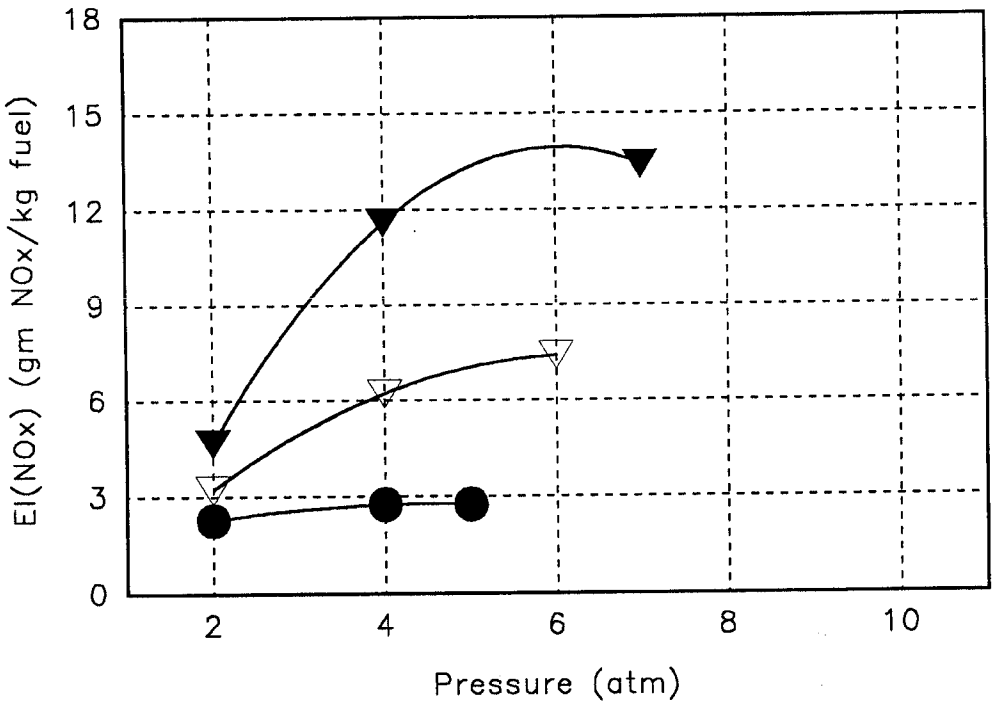

Figure 5.9 - EI(NO_X) for RZ Φ = 2.0, LZ Φ = 0.4, Ref Vel = 20 m/s

A comparison of this data with that from the previous set (where the lean zone equivalence ratio was maintained at 0.375) reveals the effect of increased rich zone equivalence ratio. Increasing the rich zone equivalence ratio, while increasing the lean zone equivalence ratio only slightly results in a slight decrease in the production of NO_X. This tendancy is illustrated by the 15 m/s, 700 K cases for the 2.0 and 1.5 rich zone equivalence ratio tests (Figures 5.5 and 5.8 respectively). When the combustor operates at a rich zone equivalence ratio of 1.5, $EI(NO_X)$ increases from 3.5 to 8.8 as pressure is increased from 2 to 7 atmospheres. However, when the combustor rich zone equivalence ratio is increased to 2.0, the $EI(NO_X)$ only increases from 3.3 to 7.2 over the same pressure interval. Such a decrease is due in part to the reduced gas temperature exiting the rich zone at the higher equivalence ratio. This also corresponds to a shortening of the residence time in the quick mix section where the local equivalence ratio is equal to 1.0. This decrease is most noticeable in the lower pressure cases.

As in the previous cases, the increase in NO_X production, and $EI(NO_X)$ becomes more apparent for the higher inlet temperatures. The trends involving pressure and reference velocity appear to remain the same as the earlier cases.

Rich Zone $\Phi = 2.0$, Lean Zone $\Phi = 0.5$. The increase in $EI(NO_X)$, due to rising lean zone equivalence ratio, is further illustrated as the lean zone equivalence ratio is changed to 0.5, while the rich zone equivalence ratio is held constant at 2.0. (Figures 5.10 through 5.12) Increasing the lean zone equivalence ratio from 0.4 to 0.5 results in an additional 33% increase in the resulting $EI(NO_X)$.

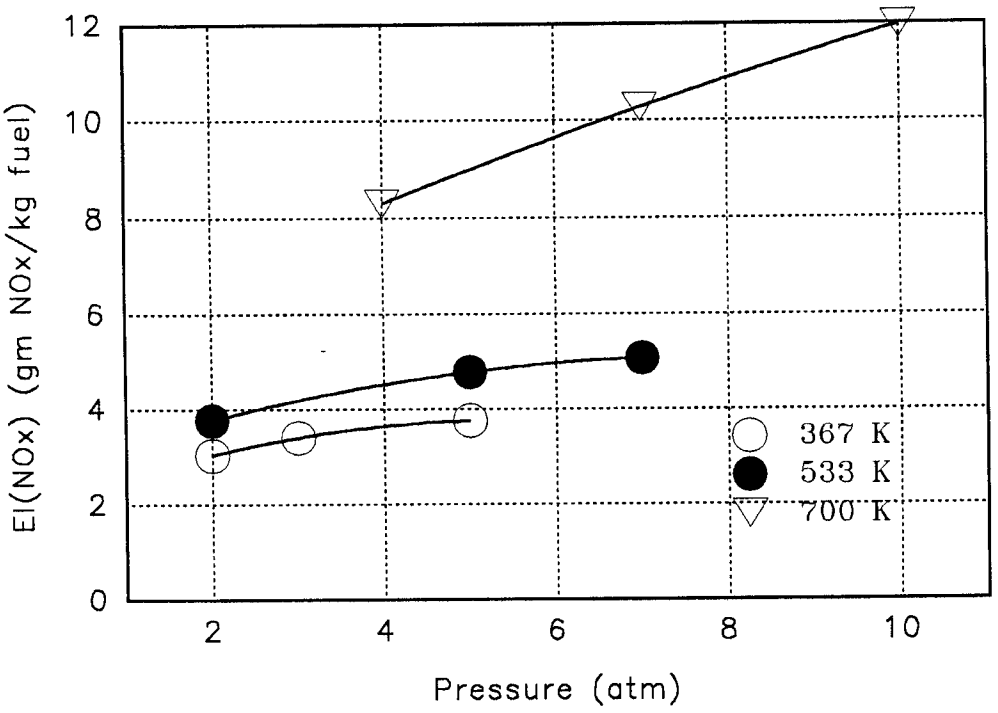

Figure 5.10 - EI(NOx) for RZ $\Phi = 2.0$, LZ $\Phi = 0.5$, Ref Vel = 10 m/s

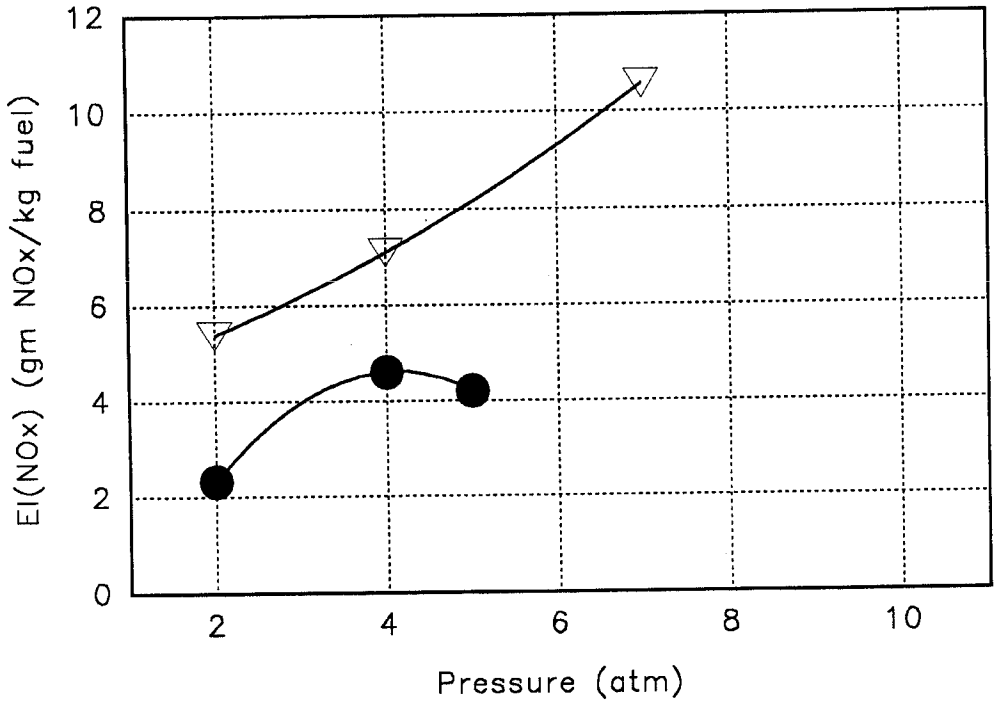

Figure 5.11 - EI(NO_X) for RZ $\Phi = 2.0$, LZ $\Phi = 0.5$, Ref Vel = 15 m/s

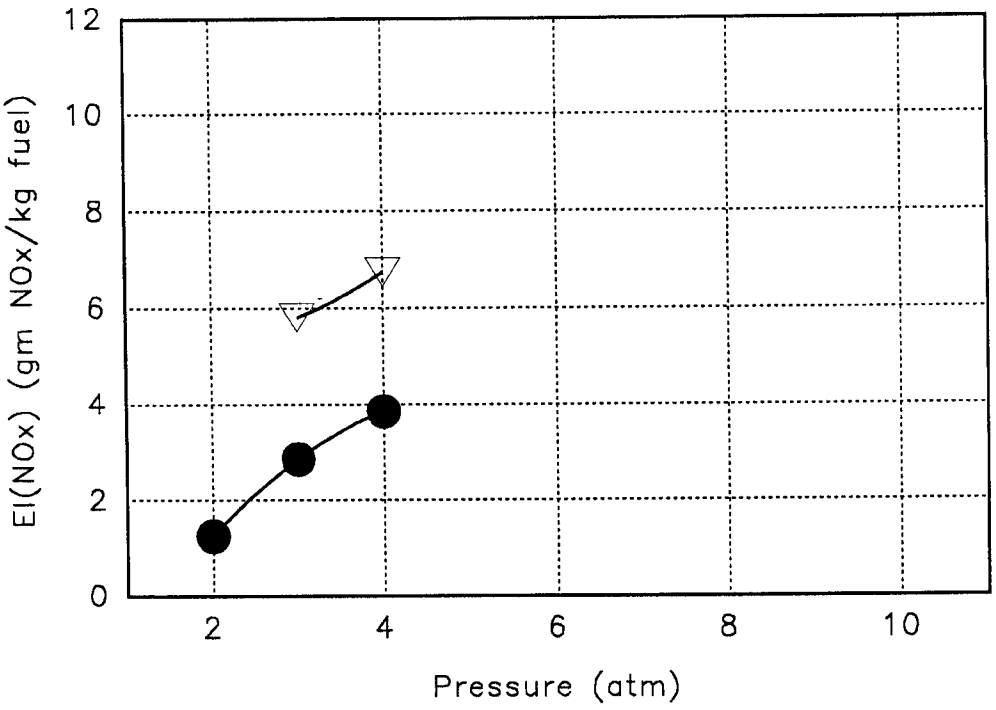

Figure 5.12 - EI(NO_X) for RZ F = 2.0, LZ F = 0.5, Ref Vel = 20 m/s

5.1.2 NO_X PRODUCTION AND REACTION TEMPERATURE

Additional insight can be gained from a comparison of EI(NO_X) to lean zone reaction temperature. For this comparison, local lean zone equivalence ratios were determined using the measured emission values and the following approximation (SAE, 1971):

$$\Phi_{lz} = [(C_{CO} + C_{CO2} + C_{UHC})M_f \times 10^{-6}]$$

$$/ [0.064 M_p n_C \{1 - {}^1/_2 \{ {}^1/_2 r(C_{CO} +$$

$$C_{CO2})x10^{-6} + C_{CO}x10^{-6}\}\}]$$

By using these computed local equivalence ratios and relating adiabatic flame temperature to inlet air temperature and equivalence ratio, (assuming Jet-A combustion with dry air for pressures from 50 kPa to 5000 kPa and equivalence ratios from 0 to 2.0), the flame temperature within the lean zone of the model combustor was computed for each of the 122 test cases. Each of these theoretical flame temperature values were then compared to their corresponding $EI(NO_X)$ values.

Figure 5.13 presents the comparison of the theoretically computed reaction temperatures with the normalized NO_X data. The data was normalized by dividing each $EI(NO_X)$ value by the largest test value recorded. The shotgun appearance of this plot, which can be attributed to the numerous varying combustion parameters, makes it complicated to draw definite conclusions. However, some insight can be gained from the quadratic least squares fit approximations for each of the four equivalence ratio combinations. These approximations point out the significant effect of reaction temperature on the rate of NO_X formation, and also suggest that rich zone equivalence ratio has an important impact on NO_X production. Increasing the rich zone equivalence ratio from 1.5 to 2.0 results in a substantial drop in $EI(NO_X)$ for a given inlet air temperature. This increase in NO_X production, accompanying the decrease of rich zone equivalence ratio, can be attributed to higher reaction temperatures, and decreased concentrations of HC radicals.

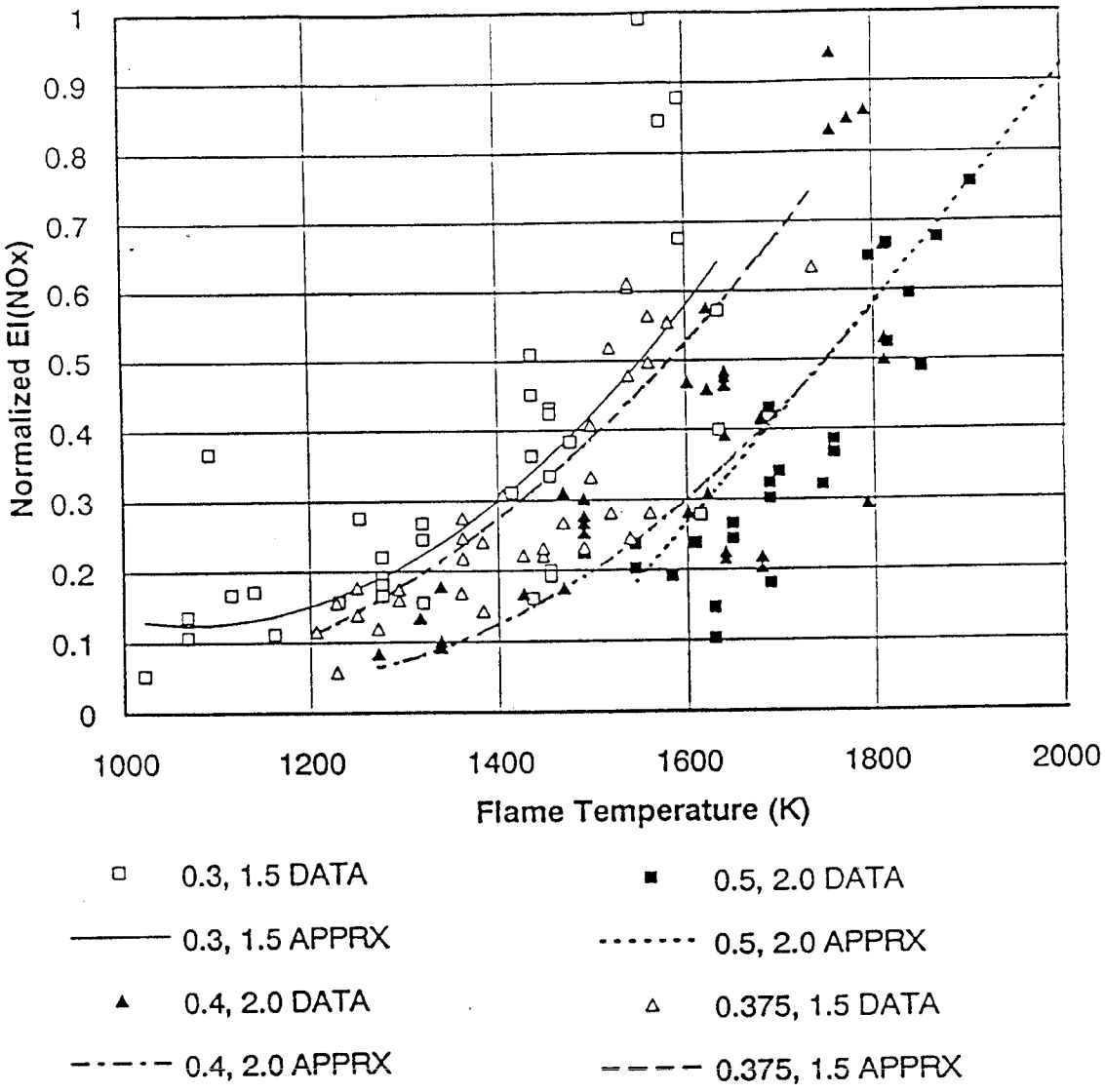

Figure 5.13 - EI(NOx) vs Reaction Temperature

5.1.3 COMBUSTION EFFICIENCY

Using measured emissions for CO, the combustion efficiency was computed with the equation (Annonymous, 1971):

$$\eta = 1 - EI(CH_{2.67}) \times 10^{-3} - 0.227 \left[EI(CO) - EI(CO)_{eq} \right] \times 10^{-3}$$

where EI(x) are the computed emissions indices for CO and UHC, which are all assumed to be of the form $CH_{2.67}$. For cases where the lean zone equivalence ratio is less than 1.0, the EI for UHC was negligible.

The resulting data (Figures 5.14 through 5.17) suggests that combustion efficiency improves with increased inlet air temperature with values of 99% being achieved for preheat air temperatures greater than 367 K. Combustion efficiency also appears to increase with residence time for cases involving lower inlet and lower lean zone equivalence ratios. For the 0.3 lean zone equivalence ratio, 367 K inlet temperature case, combustion efficiency drops to nearly 90% when the reference velocity is set to 20 m/s (Figure 5.14). Combustion efficiency increases to 97% when the reference velocity is decreased to 15 m/s. When the lean zone equivalence ratio is increased to 0.375, with inlet temperature constant at 367 K, combustion efficiency increases to 97% for a reference velocity of 20 m/s (Figure 5.15). The basis for the relationship between increased efficiency and increased lean zone equivalence ratio lies in the relationship between equivalence ratio and flame temperature. There appears to be no significant relation between combustion efficiency and pressure. These results would tend to agree with the trade off of NO_x for CO expected for typical combustion. As illustrated in Figures 5.1 and 5.14, for 367 K preheat, low NO_x production is accompanied by high CO and UHC.

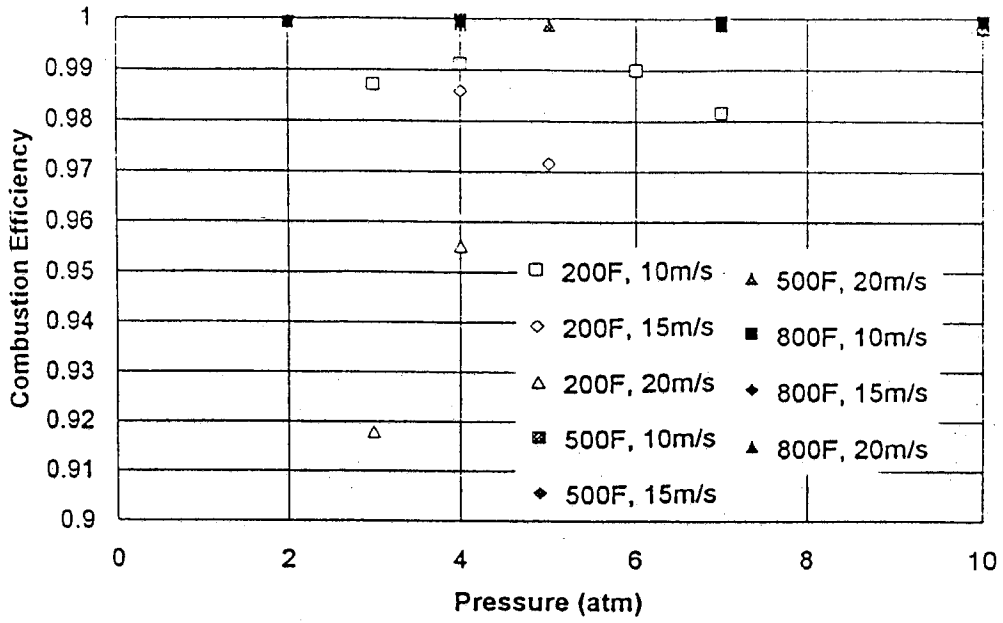

Figure 5.14 – Combustion Efficiency for 1.5 Rich Zone, 0.3 Lean Zone

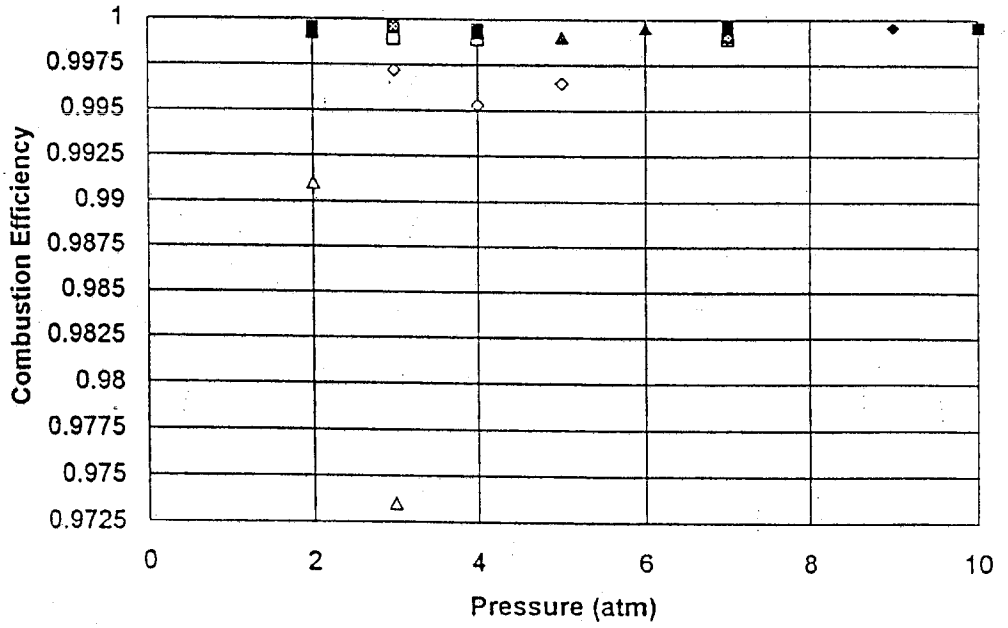

Figure 5.15 - Combustion Efficiency for 1.5 Rich Zone, 0.375 Lean Zone

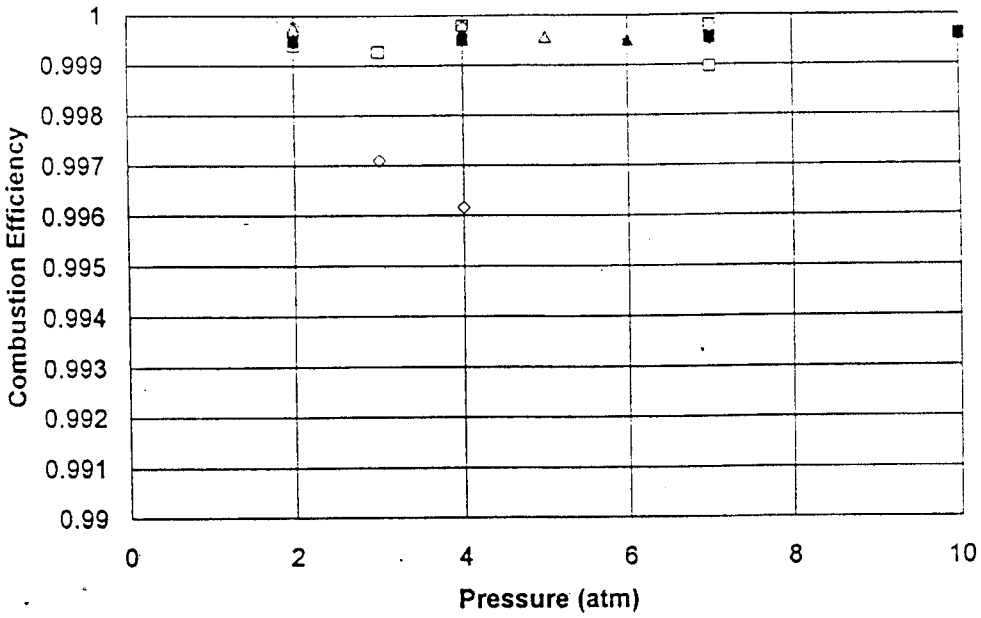

Figure 5.16 - Combustion Efficiency for 2.0 Rich Zone, 0.4 Lean Zone

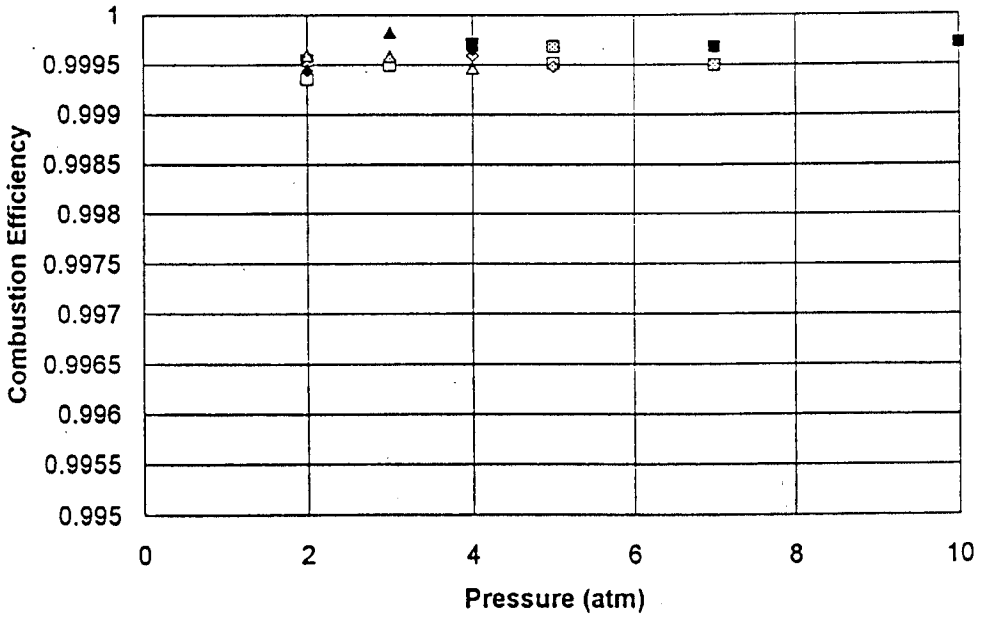

Figure 5.17 - Combustion Efficiency for 2.0 Rich Zone, 0.5 Lean Zone

5.2 PHASE 2 TESTING

5.2.1 RICH ZONE EXIT EMISSION PROFILE

The traversable emissions probe sampled emissions from the 5.0 cm diameter rich zone exit while the combustor was operated at the following conditions: T3 = 700 K, P3 = 400 kPa, reference velocity = 10 m/s, and rich zone equivalence ratio = 1.5. A 3:1 flow split was used. Therefore, the corresponding reference velocity in the rich zone was 2.5 m/s and the corresponding lean zone equivalence ratio was 0.375. The measured profiles for NO_X, CO, and UHC at the rich zone exit are presented in Figures 5.18 and 5.19.

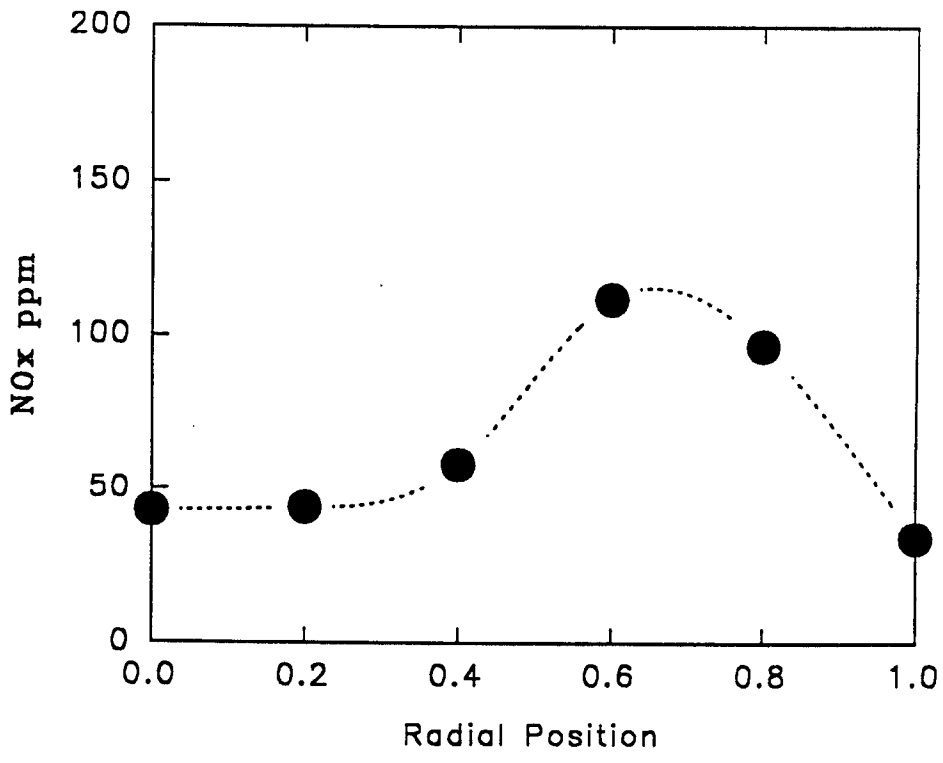

Figure 5.18 - NOx Profile at Exit of Rich Zone

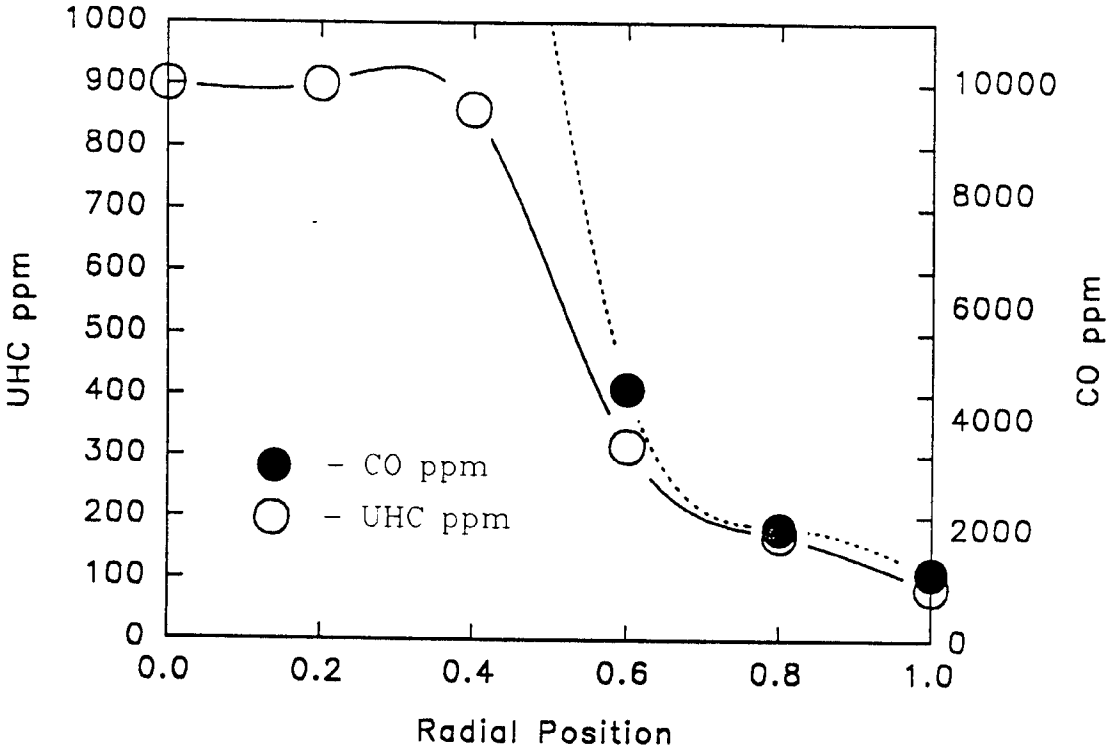

Figure 5.19 - CO and UHC Profiles at Exit of Rich Zone

Since the combustor was axis-symetric, only half of the exit was profiled. For these plots, the radial distance of the probe sample port from the rich zone exit centerline has been normalized, with 0.0 indicating the centerline and 1.0 indicating a distance 2.54 cm from the centerline (the wall).

From these profiles, two significant conclusions can be drawn. The first of these conclusions is that the mixing within the current rich zone module is not uniform. Low CO and UHC levels near the wall of the exit suggest that the reaction does not expand very far from the centerline. The NO_x spike can be attributed to a transition from a fuel rich mixture at the center of the rich zone to a fuel lean mixture at the wall.

The second conclusion that can be drawn is that a relatively small portion of the total NO_X produced in this model RQL combustor is produced in the rich zone. Exit plane measurements from Phase 1 tests revealed that, for these conditions, the model combustor produced 5.5 grams of NO_X per kilogram of fuel consuled. A reasonable approximation of the volume weighted rich zone NO_X values (made by assuming a turbulent pipe flow though the rich zone exit) suggests that only 0.88 grams of NO_X is produced in the rich zone per kilogram of fuel consumed. This accounts for only 16% of the total NO_X produced.

5.2.2 LEAN ZONE ENTRANCE EMISSION PROFILE

The traversable emissions probe also sampled emissions from the 5.0 cm diameter lean zone entrance. The same operating conditions were used as for the rich zone emission profile test: T3 = 700 K, P3 = 400 kPa, reference velocity = 10 m/s, rich zone equivalence ratio = 1.5, and lean zone equivalence ratio = 0.375.

The measured profiles for NO_X, CO, and UHC at the lean zone entrance are presented in Figures 5.20 and 5.21. Again, because of symmetry, only half of the entrance was profiled. Similar to the plots in Figures 5.18 and 5.19, the radial distance of the probe sample port from the lean zone entrance centerline has been normalized, with 0.0 indicating the centerline and 1.0 indicating a distance 2.54 cm from the centerline (the wall).

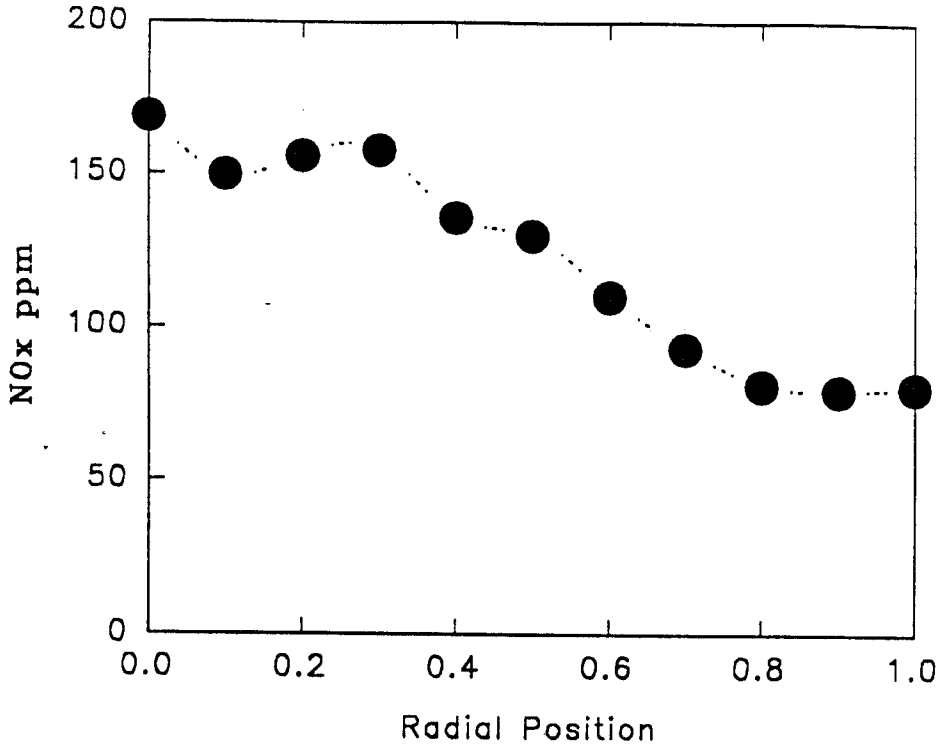

Figure 5.20 - NO_X Profile at Entrance of Lean Zone

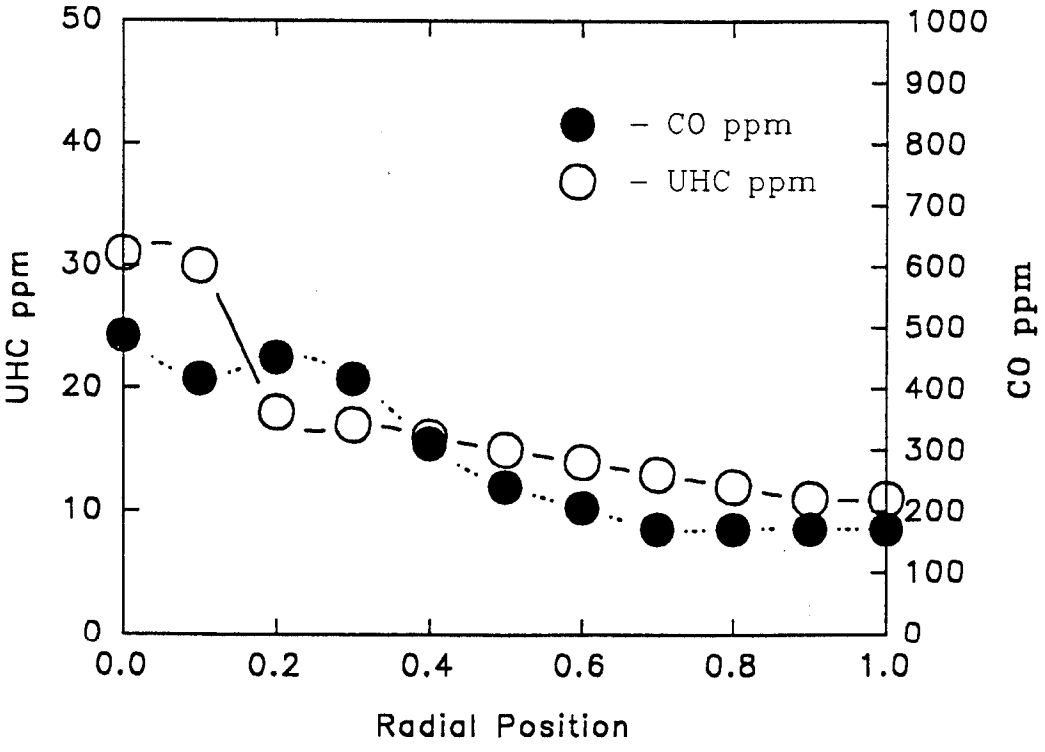

Figure 5.21-CO and UHC Profiles at Entrance of Lean Zone

Two significant conclusions can also be drawn from these profile. The first of these conclusions is that the combustion efficiency increases almost immediately following the quick mix dilution jets. CO and UHC levels are both an order of magnitude lower than those from the rich zone exit.

The second conclusion that can be drawn is that a the bulk of the NOx produced in this model RQL combustor is produced in the quick mix module. By again assuming that the flow into the lean zone is turbulent, an approximation of the volume weighted lean zone entrance NO_X values can be made. This approximation suggests that only 0.76 grams of NO_X is produced in the lean zone per kilogram of fuel consumed. This accounts for less than 14% of the total NO_X produced. Thus, over 70% of the total NO_X formed is produced in the quick mix module.

6.0 SUMMARY AND CONCLUSIONS

6.1 SUMMARY

This research examined the role inlet temperature, pressure, reference velocity, rich zone equivalence ratio, and lean zone equivalence ratio play in the production of emissions from a model rich burn - quick mix - lean burn combustor in the fuel rich zone (first stage) and the fuel lean zone (third stage). The first task of the research involved modifying an existing testing facility in order to make it capable of simulating actual gas turbine engine combustor operating conditions. The second task of the research involved the development of a model RQL combustor that would simulate the plenum air feed of real gas turbine engines. The third task of the research involved the acquisition of emissions data from the model combustor operated at realistic conditions. This task was divided into four parts: experimental development, flow splits tests, Phase 1 emissions testing, and Phase 2 emissions testing.

During the experimental development, operating parameters to be examined in relation to NO/NO_X emissions were selected. During the flow splits testing, the plenum feeding of the model RQL combustor was examined and characterized. During the Phase 1 testing the influence of several operating parameters on NO_X emissions and combustion efficiency were evaluated. And finally, during the Phase 2 testing, emission profiles were obtained in the rich zone exit and lean zone entrance of the model combustor, while the combustor was operated at realistic conditions.

Emission profiles at the rich zone exit and lean zone entrance revealed that the bulk of the NO_X formed in the model RQL combustor was

produced in the quick mix module. The profiles also revealed that mixing within the rich zone module was not uniform.

6.2 CONCLUSIONS

From the measured emissions data, several conclusions can be drawn.

- NOx production in an RQL can combustor, operating at fixed inlet air temperature and pressure, can be minimized by: decreasing lean zone equivalence ratio, increasing rich zone equivalence ratio, and decreasing lean zone residence time.

- NO_X production increases with operating pressure to the 0.4 power. Also, as expected, NO_X production increases with increasing inlet air temperature.

- Combustion efficiency can be maximized by: increasing inlet air temperature, increasing operating pressure and increasing overall residence time. For the RQL combustor operating with inlet air preheat temperatures greater than 367 K, combustion efficiency will exceed 99%.

- The rich zone is not uniform and accounts for on the order of 16% of the total NO_X produced.

REFERENCES

Allen, L. and Slusher, G.R., "Ambient Temperature and Humidity Factors for Exhaust Emissions from Two-Classes of Aircraft Turbine Engines," FAA-RD-76-149, AD A031923, October 1976, National Aviation Facilities Experimental Center, Atlantic City, NJ

Anderson, D.N., "Effects of Equivalence Ratio and Dwell Time on Exhaust Emissions from an Experimental Premixing Prevaporizing Burner," ASME Paper 75-GT-69, 1975

Annonymous, Procedures for the Continuous Sampling and Measurement of Gaseous Emissions from Aircraft Turbine Engines. Aerospace Recommended Practice 1256, SAE, 1971.

Brady, R.A., "A Study of Dome Region Fuel-Air Mixing in a Model Rich Burn - Quick Mix -Lean Burn Combustor," MS Thesis, UCI, 1991.

Bryce, G.R., "Data Analysis in RUMMAGE - A User's Guide," Brigham Young University, Statistics Department, Provo, UT (1980)

Beér, J.M., Jacques, M.T., Farmayan, W.F., Gupta, A,K., and Hanson, S., "Reduction of NO_X and Solid Emissions By Staged Combustion of Coal Liquids Fuels," *19th Symposium on Combustion*, The Combustion Institute, 1982, pp. 1301-1309

Donovan, P. and Cackette, T., "The Effects of Ambient Conditions on Gas Turbine Emissions - Generalized Correction Factors," ASME Paper No. 78-GT-87

Drennan, S.A., "The Development of a High Pressure Nozzle Characteristion Facility with Optical Access," Master's Thesis, UCI Combustion Laboratory Report ARTR-90-7, University of California, Irvine, 1990

Drennan, S.A., Peterson, C.O., Khatib, F.M., Sowa, W.A., Samuelsen, G.S., "Pollutant Emissions From and Within a Model Gas Turbine Combustor at Elavated Pressures and Temperatures," UCI Combustion Laboratory, University of California, Irvine, 1993

Drennan, S.A., Sowa, W.A., and Samuelsen, G.S., "The Effects of Ambient Pressure on the Spray Characteristics of a Twin-Fluid Atomizer," 1990, ASME Paper 90-GT-393

Fenimore, C.P., *13th Symposium on Combustion,* The Combustion Institute, 1971, p. 373

Fenimore, C.P., Drake, M.C., Correa, S.M., Pitz, R.W., and Shyy, W., "Superequilibrium and Thermal Nitric Oxide Formation in Turbulent Diffusion Flames", Combustion and Flame 69, pp. 347-365, 1987

Fowler, J, Honnery, D., "The Influence of Pressure on NOx Production from Turbulent H2-Air Diffusion Flames," Western States Section of the Combustion Institute, Paper 93-041, 1993

Gardiner, W.C., *Combustion Chemistry*, Springer-Verlag, New York, 1987

Grove, J.W., and Samuelsen, G.S., "Transformation of Nitrogen Oxides While Sampling Combustion Products," University of California, Irvine, 1984

Glassman, I., *Combustion, Second Edition*, Academic Press, Orlando, 1987.

Haynes, B.S., Iverach, D., and Kirov, N.Y., *15th Symposium on Combustion*, The Combustion Institutem 1975, p. 1103

Herberling, P.V., "Prompt NO" Measurements at High Pressures, *16th Symposium on Combustion*, The Combustion Institute, 1976, pp. 159-168

Hori, Morio, "Experimental Study of NO2 Formation in Combustion Systems," *21st Symposium on Combustion*, The Combustion Institute, 1986, pp. 1181-1188

ICAO, *US Extension of the ICAO Standard Atmosphere*, 1958

Iverach, D., Basden, K.S., and Kirov, N.Y., "Formation of Nitric Oxide in Fuel-Lean and Fuel Rich Flames," *14th Symposium on Combustion*, The Combustion Institute, 1974, pp. 767 -775

Johnston, H., "Reduction of Stratospheric Ozone by Nitrogen Oxide Catalysts from Supersonic Aircraft Exhaust," *Science*, Vol. 173, 1971, pp. 517-521

Jones, Robert E.; Trout, Arthur M., Wear, Jerrold D., McBride, Bonnie J., "Combustion Gas Properties: I-ASTM Jet A Fuel and Dry Air," Lewis Research Center, Cleveland, OH, 1984.

Lefebvre, A.H., *Gas Turbine Combustion*, Hemisphere Publishing, New York, 1983

Lipfert, F.W., "Correlation of Gas Turbine Emissions Data," ASME Paper No. 72-GT-60

Martel, Charles, R., "Molecular Weight and Average Composition of JP-4, JP-5, JP-8 and Jet-A", AFWAL/POSF, 1988

Martin, F.J., and Dederick, P.K., "NOx From Fuel Nitrogen in Two-Stage Combustion," *16th Symposium on Combustion*, The Combustion Institute, 1976, pp. 191- 198

Mattingly, Jack D., Heiser, William H., Daley, Daniel H., *Aircraft Engine Design*, American Institute of Aeronautics and Astronautics, Inc., 1987, pp. 332,333

Miller, James A., and Bowman, Craig T., "Mechanism and Modeling of Nitrogen Chemistry in Combustion," *Progress in Energy and Combustion Science*, 1991

Mosier, S.A., Pierce, R.M., Smith, C.E., and Hinton B.S., "Advanced Combustor Systems for Stationary Gas Turbines," Final Report FR 11405, Contract No. 68-02-2136, U.S. Environmental Protection Agency, 31 March, 1980

Natarajan, K., and Roth, P., "A Shock Tube Study of CN Radical Reactions with H2 and NO Verified by H, N, and O Atom Measurements," *21st Symposium on Combustion*, The combustion Institute, 1986, pp. 729-737

Odgers, J., "Current Theories of Combustion Within Gas Turbine Chambers," *15th Symposium on Combustion*, The Combustion Institute, 1974

Odgers, J., and Kretschmer, D., *The Design and Development of Gas Turbine Combustors - Volume 1, Northern Research and Engineering Corporation*, Woburn, Mass., 1980, p. 1.27

Peterson, C.R., and Hill, P.G., *Mechanics and Thermodynamics of Propulsion*, Addison-Wesley, Mass, 1965, pp. 157,158

Pratt & Whitney Operating Instructions 200, *The Aircraft Gas Turbine Engine and its Operation*, United Technologies Corporation, 1988

Sadakata, M., Fujioka, Y., and Kunii, D., "Effects of Air Preheating on Emissions of NO, HCN, and NH3 from Two-Stage Combustion," *18th Symposium on Combustion*, The Combustion Institute, 1981, pp. 65-72

Semerjian, H., and Vranos, A., "NOx Formation in Turbulent Premixed Flame," *16th Symposium on Combustion*, The Combustion Institute, 1976, pp. 169-178

Samuelsen, G.S., "The Combustion Aspects of Air Pollution," *Advances in Environmental Science and Technology*, Wiley, New York, NY, pp. 219-322, 1975.

Smith, I.E., *Combustion in Advanced Gas Turbine Systems*, Proceedings of an International Propulsion Symposium held at the College of Aeronautics, Cranfield, 1968

Szekely, A., Hanson, R.K., and Bowman, C.T., International Journal of Chemical Kinetics. No 15, p 915, 1983

Personal Communication with Charles Westbrook, Sept, 1992

Yamagishi, Kazuo, Nozawa, Masaaki, Yoshie, Terukazu, Tokumoto, Tsunenori, and Kakegawa, Yasuo, "A Study of NOx Emissions Characteristics in Two-Stage Combustion," *15th Symposium on Combustion*, The Combustion Institute, pp.1157-1166, 1975

Zeldovich, J., "The Oxidation of Nitrogen in Combustion and Explosions," *Acta Physicochimica*, URSS, Vol. 21, 4, pp. 577-628., 1946.

APPENDIX A: EI(NO_X) EQUATION DERIVATION

The equation used to convert the measured ppm value for NO_X to the corresponding emissions index was derived in the following manner:

By definition:

$$EI(NO_X) = (\text{grams of } NO_X \text{ produced / kg of fuel consumed})$$

Grams of NO_X can be expressed in terms of ppm NO_X using the following equation:

$$\text{grams } NO_X = \text{ppm } NO_X \left[(MW\ NO_X / MW\ \text{exhuast})\right] \text{ grams of exhaust}$$

Since the ppm measurements are recorded based on a dry sample volume, they must be corrected to account for the volume of condensed water.

$$EI(NO_X) = (MW_{NO_X}/MW_{\text{dry exhaust}}) \left[(100 - \%H_2O)/100\right]$$
$$(\text{grams of exhaust / kg of fuel consumed})\ NO_X \text{ ppm}$$

For this thesis, the % of NO_X that was NO was greater than 90%. The convention, however, is that the molecular weight of NO_X is that of NO_2. Therefore:

$$EI(NO_X) = (MW_{NO_2}/MW_{\text{dry exhaust}}) \left[(100 - \%H_2O)/100\right]$$
$$(\text{grams of exhaust / kg of fuel consumed})\ NO_X \text{ ppm}$$

APPENDIX B: EMISSIONS ANALYZERS

Thermo Electric Model 10A Chemiluminescent NO/NO_x Analyzer

In the NO/NO_x analyzer, the chemiluminescent reaction of NO and O_3 provided the basis for the analysis. Specifically,

$$NO + O_3 \rightarrow NO_2 + O_2 + hv$$

Light emission results when electronically excited NO_2 molecules revert to their ground state.

To measure NO concentrations, the gas sample to be analyzed was blended with O_3 in a reaction chamber. The resulting chemiluminescence was monitored through an optical filter by a high-sensitivity photomultiplier positioned at one end of the chamber. The filter/photomultiplier combination responded to light in a narrow-wavelength band unique to the above reaction (hence, no interference). The output from the photomultiplier was linearly proportional to the NO concentration.

To measure NO_x concentrations (i.e., NO plus NO_2), the sample gas flow was diverted through to an NO_2 to NO converter. The chemiluminescent response in the reaction chamber to the converter effluent was linearly proportional to the NO_x concentration entering the converter.

Beckman Model 755 O_2 Analyzer

The Beckman Industrial Model 755 O_2 analyzer measured the magnetic susceptibility of the sample gas. O_2 is strongly paramagnetic.

Other gases, with few exceptions, are weakly diamagnetic. Of these exceptions, none constitute a substantial component of combustion exhaust.

Horiba Model PIR 2000 CO/CO_2 Analyzers

The Horiba Model PIR 2000 analyzers continuously determined the concentration change of CO and CO_2 by measuring the infrared absorption specific to the species of interest. Both of these molecules absorb infrared radiation of a specific wavelength and the degree of absorption is proportional to the concentration at constant pressure.

More specifically, the Horiba analyzers used the following design. Infrared radiation was emitted from a light source and passed through a sample cell containing emissions sample and a reference cell containing air. After passing through the cells, the radiation was modulated by a rotating chopper. If a portion of the infrared radiation passing through the sample cell was absorbed by the sample gas, a decrease in amount of radiation reaching the sample side of the detector would result. This difference caused a membrane between the sample and reference cells in the detector to produce an electrical output which was amplified and directed to a meter.

Horiba MEXA-554GE and Hot FID, Model 1120 TRI-F UHC Analyzers

The first of the hydrocarbon detectors, the MEXA-554GE table top analyzer, was loaned to UCI by Horiba. This Model's primary designed usage is in the auto smog servicing industry.

The second hydrocarbon analyzer was the Horiba Hot FID, Model 1120 TRI-F. This unit measured the concentration of the total hydrocarbons present in a sample of gas by means of a hydrogen flame ionization detector, or FID. The principle of the hydrogen flame ionization detection

method is that if a trace amount of hydrocarbons is introduced into a hydrogen flame within the analyzer, the hydrocarbons decompose by the high temperature energy of the flame. As a result of this reaction, a number of ions proportional to the number of carbon atoms are generated. By applying a direct voltage across the flame and placing a collective electrode around the flame, ions are collected. In this manner, the current proportional to the number of carbon atoms is passed through the collective electrode and is processed as a signal. The hydrogen flame ionization detection method is least sensitive to inorganic gases (such as CO, CO_2, NO, NO_2, SO_2, and N_2) which normally coexist in the sample.

APPENDIX C: DATA FROM RUMMAGE II

The Rummage II linear regression program (Bryce, 1980) used to analyze the data from the Phase 1 testing assumes the operating parameters of the model RQL combustor (inlet pressure, inlet temperature, reference velocity, rich zone equivalence ratio and lean zone equivalence ratio) can be related to the computed EI(NOx) value by the following equation:

$$\ln[EI(NO_x)] = C_1\ln(P3) + C_2\ln(T3) + C_3\ln(\text{Ref Vel}) + C_4\ln(\Phi_{rz}) + C_5\ln(\Phi_{lz})$$

Where C_1, C_2, C_3, C_4, and C_5 are constants determined to fit the data. This equation can be expressed in the following form:

$$\ln(EI(NO_x)) = \ln(P3^{C1} * T3^{C2} * \text{Ref Vel}^{C3} * \Phi_{rz}{}^{C4} * \Phi_{lz}{}^{C5})$$

Taking the exponential from both sides reveals:

$$EI(NOx) = P3^{C1} * T3^{C2} * \text{Ref Vel}^{C3} * \Phi_{rz}{}^{C4} * \Phi_{lz}{}^{C5}$$

The constants computed by Rummage were:

$C_1 = 0.42$

$C_2 = 0.77$

$C_3 = -0.51$

$C_4 = -1.51$

$C_5 = 1.84$

1.5,0.375

SOURCE	VARIABLE NO.	ESTIMATED LINEAR COMBINATIONS	STD. ERR.	SUM OF SQUARES	F-RATIO	P LEVEL
MEAN	1	-51.488485	22.900380	14.063856	5.055159	0.031
C1	2	0.064636	0.031292	11.870061	4.266614	0.047
C3	3	-0.000018	0.000011	7.646052	2.748322	0.107

2.0,0.5

SOURCE	VARIABLE NO.	ESTIMATED LINEAR COMBINATIONS	STD. ERR.	SUM OF SQUARES	F-RATIO	P LEVEL
MEAN	1	-24.200256	47.898721	0.641523	0.255265	0.618
C1	2	0.011367	0.053768	0.112318	0.044692	0.834
C3	3	0.000004	0.000015	0.143619	0.057147	0.813

1.5,0.3

SOURCE	VARIABLE NO.	ESTIMATED LINEAR COMBINATIONS	STD. ERR.	SUM OF SQUARES	F-RATIO	P LEVEL
MEAN	1	31.950017	26.044994	11.031200	1.504852	0.229
C1	2	-0.055838	0.039452	14.683947	2.003151	0.167
C3	3	0.000026	0.000015	23.187545	3.163193	0.085

2.0,0.4

SOURCE	VARIABLE NO.	ESTIMATED LINEAR COMBINATIONS	STD. ERR.	SUM OF SQUARES	F-RATIO	P LEVEL
MEAN	1	27.227857	38.743349	2.670300	0.493893	0.487
C1	2	-0.046042	0.049886	4.605470	0.851818	0.362
C3	3	0.000020	0.000016	8.794852	1.626676	0.210

```
-- MODEL Y = C15+C13+C10+C11+C12+E
*
-- LOGE C2 C13
LOGE  OF  C2  PUT INTO  C13

*
-- LOGE C3 C10
LOGE  OF  C3  PUT INTO  C10

*
-- LOGE C5 C12
LOGE  OF  C5  PUT INTO  C12

*
-- LOGE C6 C14
LOGE  OF  C6  PUT INTO  C14

*
-- LOGE C1 C15
LOGE  OF  C1  PUT INTO  C15

*
-- DEPE C14
*
-- NO CONST
*
-- LAST
*
-- READ C1-C9
     C1          C2          C3          C4          C5          C6          C7          C8          C9
     C11         C12         C13         C14         C15
```

2.00000	0.40000	9.00000	1100.00000	15.00000	14.89000	1.34000	0.00000	0.99970
7.00307	2.70805	-0.91629	2.70069	0.69315				
2.00000	0.40000	2.00000	1100.00000	20.00000	4.65000	1.67000	0.00000	0.99960
7.00307	2.99573	-0.91629	1.53687	0.69315				
2.00000	0.40000	4.00000	1100.00000	20.00000	13.60000	1.69000	0.00000	0.99960
7.00307	2.99573	-0.91629	2.61007	0.69315				
2.00000	0.40000	7.00000	1100.00000	20.00000	13.41000	1.33000	0.00000	0.99970
7.00307	2.99573	-0.91629	2.59600	0.69315				

ONUMBER OF DATA RECORDS READ = 122
ONUMBER OF DATA RECORDS USED = 122
OSAMPLE SIZE = 122

OCOL	MEAN	VAR.	STD DEV	MIN	MAX
1	1.73361	0.06275	0.25049	1.50000	2.00000
2	0.38730	0.00456	0.06752	0.30000	0.50000
3	4.54918	5.30748	2.30380	2.00000	10.00000
4	632.78689	**********	296.38110	200.00000	1100.00000
5	14.63115	15.77191	3.97139	10.00000	20.00000
6	5.55803	12.74976	3.57068	0.83000	17.48000
7	11.75713	1662.90414	40.77872	0.76000	361.45001
8	0.23738	0.53294	0.73003	0.00000	5.94000
9	0.99703	0.00010	0.00995	0.91300	1.00000
10	1.38615	0.26595	0.51571	0.69315	2.30259
11	6.31000	0.32948	0.57401	5.29832	7.00307
12	2.64531	0.07771	0.27877	2.30259	2.99573
13	-0.96348	0.03000	0.17322	-1.20397	-0.69315
14	1.51985	0.40519	0.63654	-0.18633	2.86106
15	0.53987	0.02077	0.14412	0.40547	0.69315

THE MODEL FOR THIS ANALYSIS IS
Y=C15 + C13 + C10 + C11 + C12 + E

1THE DEPENDENT VARIABLE FOR THIS TABLE IS C14

SEQUENTIAL ANALYSIS OF VARIANCE TABLE Tue Apr 13 16:45:10 1993

SOURCE	DF	SUM OF SQUARES	MEAN SQUARES	EXPECTED MEAN SQUARE COEFF. C15	C13	C10	C11	C12
C15	1	272.832300	272.832300	38.072	98.200	217.421	4559.386	795.718
C13	1	8.743271	8.743271	0.000	18.682	17.403	278.131	53.918
C10	1	10.751462	10.751462	0.000	0.000	31.770	0.701	0.258
C11	1	24.848095	24.848095	0.000	0.000	0.000	59.220	3.696
C12	1	2.506865	2.506865	0.000	0.000	0.000	0.000	9.531
REGR.	5	319.681992	63.936398					
ERROR	117	11.160724	0.095391					
TOTAL(C)	122	330.842712						
TOTAL	122	330.842712						

SIMPLE R-SQUARED = 0.966
R-SQUARED ADJUSTED FOR D.F. = 0.965

0STD. DEV. = 0.308854
1THE DEPENDENT VARIABLE FOR THIS TABLE IS C14
Tue Apr 13 16:45:10 1993

SOURCE	VARIABLE NO.	ESTIMATED LINEAR COMBINATIONS	STD. ERR.	SUM OF SQUARES	F-RATIO	P LEVEL
C15	1	-1.512043	0.240928	3.757162	39.387043	0.000
C13	2	1.843974	0.193642	8.650002	90.679619	0.000
C10	3	0.420271	0.056569	5.265079	55.194828	0.000
C11	4	0.775891	0.047281	25.687894	269.291107	0.000
C12	5	-0.512870	0.100045	2.506865	26.279945	0.000

* ABOVE ESTIMATES ARE ONLY EASILY INTERPRETED FOR FIXED MODELS USING ORTHOGONAL CONTRASTS WITH NO MISSING CELLS
1THE DEPENDENT VARIABLE FOR THIS TABLE IS C14

ADJUSTED ANALYSIS OF VARIANCE TABLE Tue Apr 13 16:45:10 1993

SOURCE	DF	SUM OF SQUARES	MEAN SQUARES	EXPECTED MEAN SQUARE COEFF. C15	C13	C10	C11	C12
C15	1	3.757162	3.757162	1.643	0.000	0.000	0.000	0.000
C13	1	8.650002	8.650002	0.000	2.544	0.000	0.000	0.000
C10	1	5.265079	5.265079	0.000	0.000	29.809	0.000	0.000
C11	1	25.687894	25.687894	0.000	0.000	0.000	42.670	0.000
C12	1	2.506865	2.506865	0.000	0.000	0.000	0.000	9.531
ERROR	117	11.160724	0.095391					

1THE DEPENDENT VARIABLE FOR THIS TABLE IS C14

0ADJUSTED HYPOTHESIS TESTS

SOURCE	DF	F-RATIO			SIGN. LEVEL
0C15	1	3.757162			
ERROR	117	0.095391	=	39.387043	0.000
0C13	1	8.650002			
ERROR	117	0.095391	=	90.679619	0.000
0C10	1	5.265079			
ERROR	117	0.095391	=	55.194828	0.000
0C11	1	25.687894			
ERROR	117	0.095391	=	269.291107	0.000
0C12	1	2.506865			
ERROR	117	0.095391	=	26.279945	0.000

1THE DEPENDENT VARIABLE FOR THIS TABLE IS C14
0THE FOLLOWING RESIDUALS WERE RELATIVELY LARGE
GREATER THAN 1.60 TIMES THEIR STD. DEV.
0

+	1.4748	2.0370	-0.562275	0.0291	-1.847581	2.8
42						
+	0.8416	1.3981	-0.556511	0.0352	-1.834459	2.8
45						
+	0.4824	1.2505	-0.768108	0.0511	-2.553075	5.3
58						
+	2.4275	1.8623	0.565163	0.0577	1.885089	2.9
85						
+	2.5938	2.0294	0.564388	0.0311	1.856451	2.9
86						
+	2.8611	2.1350	0.726064	0.0389	2.397872	4.7
88						
+	2.3712	1.6466	0.724538	0.0252	2.376015	4.7
89						
+	2.6319	1.8818	0.750059	0.0315	2.467749	5.0
116						
+	2.1282	1.5984	0.529867	0.0425	1.753297	2.5
121						
+	2.6101	1.7421	0.867940	0.0167	2.833960	6.7
122						
+	2.5960	1.9773	0.618680	0.0255	2.029137	3.4

0NUMBER OF INTERIOR STD. RESIDUALS 108
NUMBER OF LARGE STD. RESIDUALS 14
NUMBER OF UNDEFINED STD. RESIDUALS 0
NUMBER OF ZERO STD. RESIDUALS 0

1Tue Apr 13 16:45:10 1993

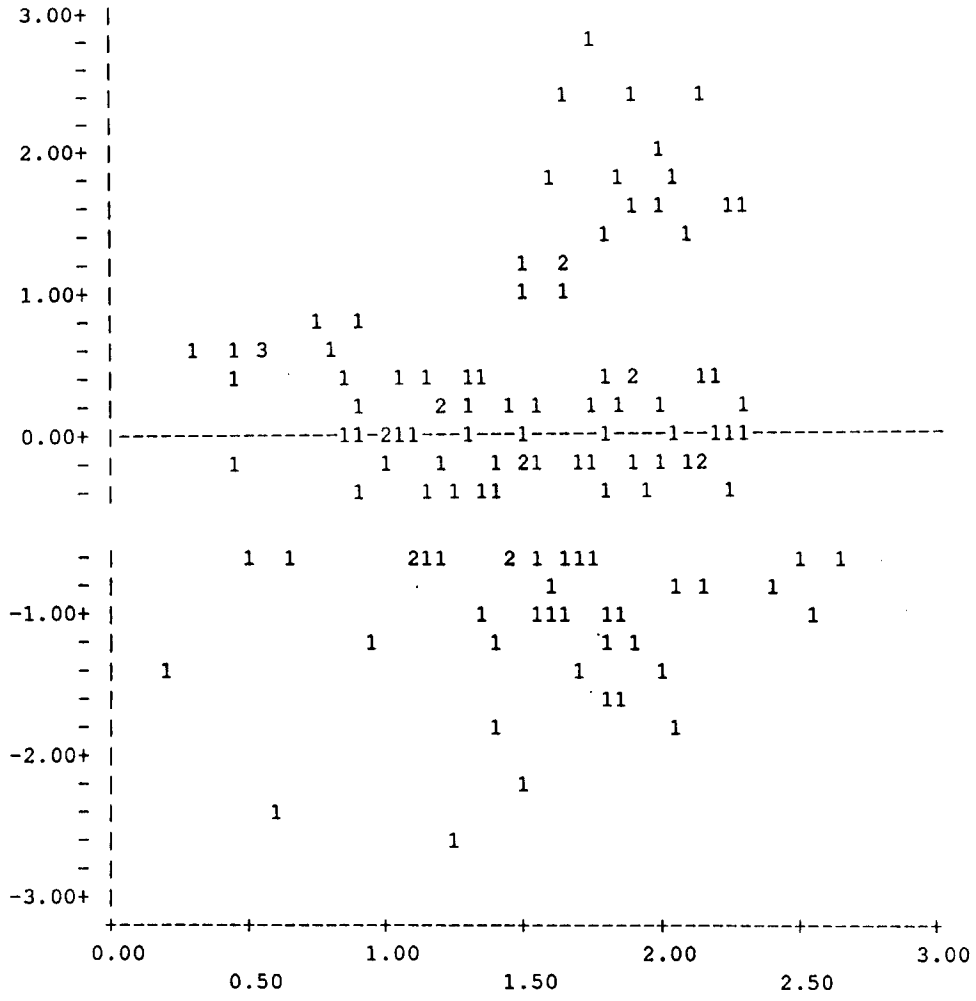
3.00+
2.00+
1.00+
0.00+
-1.00+
-2.00+
-3.00+
0.00
0.50
1.00
1.50
2.00
2.50
3.00

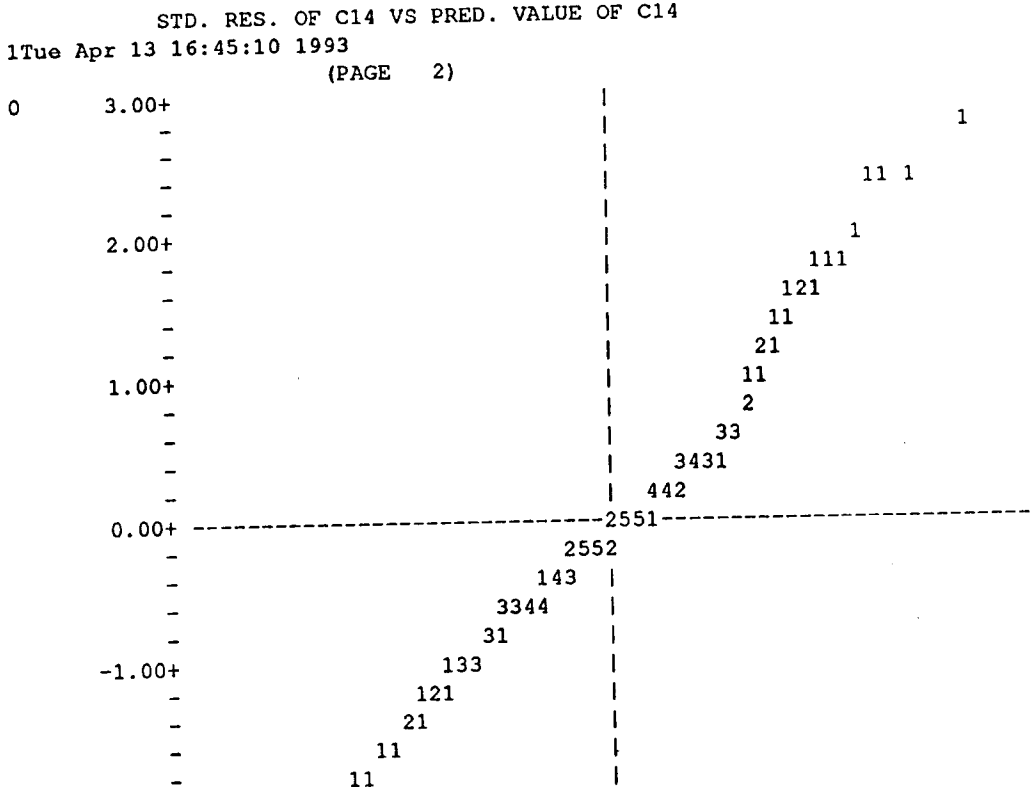
STD. RES. OF C14 VS PRED. VALUE OF C14
1Tue Apr 13 16:45:10 1993
(PAGE 2)
0
3.00+
2.00+
1.00+
0.00+
-1.00+
1
11 1
1
111
121
11
21
11
2
33
3431
442
2551
2552
143
3344
31
133
121
21
11
11

REPORT DOCUMENTATION PAGE

Form Approved
OMB No. 0704-0188

1. AGENCY USE ONLY (*Leave blank*)	2. REPORT DATE	3. REPORT TYPE AND DATES COVERED
	December 2002	Final Contractor Report

4. TITLE AND SUBTITLE

Performance of a Model Rich Burn-Quick Mix-Lean Burn Combustor at Elevated Temperature and Pressure

5. FUNDING NUMBERS

WBS–22–714–02–08
NAG3–1110

6. AUTHOR(S)

Christopher O. Peterson, William A. Sowa, and G.S. Samuelsen

7. PERFORMING ORGANIZATION NAME(S) AND ADDRESS(ES)

University of California, Irvine
Irvine, California 92697–3550

8. PERFORMING ORGANIZATION REPORT NUMBER

E–13663

9. SPONSORING/MONITORING AGENCY NAME(S) AND ADDRESS(ES)

National Aeronautics and Space Administration
Washington, DC 20546–0001

10. SPONSORING/MONITORING AGENCY REPORT NUMBER

NASA CR—2002-211992

11. SUPPLEMENTARY NOTES

Project Manager, Robert R. Tacina, Turbomachinery and Propulsion Systems Division, NASA Glenn Research Center, organization code 5830, 216–433–3588.

12a. DISTRIBUTION/AVAILABILITY STATEMENT

Unclassified - Unlimited
Subject Category: 07 Distribution: Nonstandard

Available electronically at http://gltrs.grc.nasa.gov

This publication is available from the NASA Center for AeroSpace Information, 301–621–0390.

12b. DISTRIBUTION CODE

13. ABSTRACT ***(Maximum 200 words)***

As interest in pollutant emission from stationary and aero-engine gas turbines increases, combustor engineers must consider various configurations. One configuration of increasing interest is the staged, rich burn - quick mix - lean burn (RQL) combustor. This report summarizes an investigation conducted in a recently developed high pressure gas turbine combustor facility. The model RQL combustor was plenum fed and modular in design. The fuel used for this study is Jet-A which was injected from a simplex atomizer. Emission (CO_2, CO, O_2, UHC, NO_x) measurements were obtained using a stationary exit plane water-cooled probe and a traversing water-cooled probe which sampled from the rich zone exit and the lean zone entrance. The RQL combustor was operated at inlet temperatures ranging from 367 to 700 K, pressures ranging from 200 to 1000 kPa, and combustor reference velocitites ranging from 10 to 20 m/s. Variations were also made in the rich zone and lean zone equivalence ratios. Several significant trends were observed. NO_x production increased with reaction temperature, lean zone equivalence ratio and residence time and decreased with increased rich zone equivalence ratio. NO_x production in the model RQL combustor increased to the 0.4 power with increased pressure. This correlation, compared to those obtained for non-staged combustors (0.5 to 0.7), suggests a reduced dependence on NO_x on pressure for staged combustors. Emissions profiles suggest that rich zone mixing is not uniform and that the rich zone contributes on the order of 16 percent to the total NO_x produced.

14. SUBJECT TERMS

Combustion chambers; Gas turbines; Emissions; Contaminants; Burners; Nitric oxide; Jet mixing flow

15. NUMBER OF PAGES

99

16. PRICE CODE

17. SECURITY CLASSIFICATION OF REPORT	18. SECURITY CLASSIFICATION OF THIS PAGE	19. SECURITY CLASSIFICATION OF ABSTRACT	20. LIMITATION OF ABSTRACT
Unclassified	Unclassified	Unclassified	